

Cooperative Look-Ahead Control for Fuel-Efficient and Safe Heavy-Duty Vehicle Platooning

Valerio Turri, Bart Besselink, and Karl H. Johansson, *Fellow, IEEE*

Abstract—The operation of groups of heavy-duty vehicles at a short inter-vehicular distance, known as platoon, allows one to lower the overall aerodynamic drag and, therefore, to reduce fuel consumption and greenhouse gas emissions. However, due to the large mass and limited engine power of trucks, slopes have a significant impact on the feasible and optimal speed profiles that each vehicle can and should follow. Maintaining a short inter-vehicular distance, as required by platooning, without coordination between vehicles can often result in inefficient or even unfeasible trajectories. In this paper, we propose a two-layer control architecture for heavy-duty vehicle platooning aimed to safely and fuel-efficiently coordinate the vehicles in the platoon. Here, the layers are responsible for the inclusion of preview information on road topography and the real-time control of the vehicles, respectively. Within this architecture, dynamic programming is used to compute the fuel-optimal speed profile for the entire platoon and a distributed model predictive control framework is developed for the real-time control of the vehicles. The effectiveness of the proposed controller is analyzed by means of simulations of several realistic scenarios that suggest a possible fuel saving of up to 12% for follower vehicles compared with the use of standard platoon controllers.

Index Terms—Distributed model predictive control, dynamic programming, fuel-efficient platooning, look-ahead control, optimal control, platooning, safe platooning.

I. INTRODUCTION

THE transportation of goods has been fundamental to the world economic development. The demand for freight transportation, together with the global economy, is expected to increase in the coming years. However, the transport sector is responsible for the emission of a significant amount of greenhouse gasses. In the European Union, the transport sector is responsible for roughly 21% of the total CO₂ emissions, and 26% of these emissions are directly accountable to road freight transportation [1], [2]. Furthermore, the emissions linked to surface (road and rail) freight transportation are expected to increase up to 247% in the next 40 years if no measures are taken [3]. In order to contrast this increase and the related impact on climate change, governments all

Manuscript received April 24, 2015; revised December 15, 2015; accepted February 27, 2016. Date of publication April 1, 2016; date of current version December 14, 2016. Manuscript received in final form March 9, 2016. This work was supported in part by the Knut och Alice Wallenbergs Stiftelse, in part by the European Union's Seventh Framework Programme within the COMPANION Project under Grant 610990, and in part by the Svenska Forskningsrådet Formas. Recommended by Associate Editor C. Canudas-de-wit.

The authors are with the ACCESS Linnaeus Centre, Department of Automatic Control, KTH Royal Institute of Technology, Stockholm 114 28, Sweden (e-mail: turri@kth.se; bart.besselink@ee.kth.se; kallej@kth.se).

Color versions of one or more of the figures in this paper are available online at <http://ieeexplore.ieee.org>.

Digital Object Identifier 10.1109/TCST.2016.2542044

over the world are agreeing in setting stringent limitations on greenhouse gas emissions connected to road freight transportation [4], [5]. In order to cope with these limitations, truck manufacturers are facing numerous challenges. Furthermore, the expected increase of the oil price [3] and the need for maintaining competitiveness require them to design vehicles and technologies that are increasingly fuel efficient. The fuel cost for a truck fleet owner, in fact, accounts roughly for one third of the total cost of operating a heavy-duty vehicle [6]. Therefore, even a reduction of a few percent of the fuel consumption would lead to significant savings.

An effective method to reduce fuel consumption and, consequently, greenhouse gas emissions is vehicle platooning. By operating groups of vehicles at a short inter-vehicular distance, the overall aerodynamic drag can be reduced. As about a quarter of the truck fuel consumption is related to the aerodynamic drag [7], platooning can have a large effect on fuel efficiency. Indeed, the experimental results (see [8]–[11]) have shown a reduction in fuel consumption of up to 10%. The majority of the research effort and experimental tests on fuel-efficient platooning, however, have considered the platoon driving in perfect environmental conditions, e.g., on flat roads and without traffic. In reality, platoons are expected to drive over public highways where varying topography and external traffic can have a large influence on their behavior and fuel consumption. In this paper, we present a novel control architecture for fuel-efficient and safe heavy-duty vehicle platooning that addresses the aforementioned problem.

Vehicle platooning is not a new control problem. The first works on vehicle platooning appeared in the 1960s. The main focus of these early works was the theoretical study of the dynamics of a string of vehicles with a particular attention on the study of string stability, i.e., the attenuation of disturbances in position, speed, and acceleration along the string of vehicles [12]–[14]. In the 1990s, the vehicle platooning concept received major interest again [15], where, for instance, platooning of passenger vehicles was investigated as a means to increase highway throughput. Although the environmental aspect was not the focus, noteworthy results on fuel reduction due to heavy-duty platooning have been reported [9]. These works and the related successful experimental results boosted the research on new aspects of vehicle platooning, such as safety, fuel efficiency, and user acceptance [16]–[18].

Due to the particular shape of heavy-duty vehicles, the potential for an increased fuel efficiency has been mostly studied for truck platooning [11], [19], [20]. However, in the majority of these works (see [11], [20]), the impact of external factors, such as slopes, is not taken into account. Because of

the large mass and the limited power of heavy-duty vehicles, altitude variations have a significant role on their behavior. Even small slopes produce such large longitudinal forces on trucks that they are often not able to keep constant speed during uphill segments (because of limited engine power) and during downhill segments without applying brakes (because of significant inertia). Hence, trucks commonly have to brake and therefore waste energy in order not to overcome speed limits during downhill sections. These aspects are studied for vehicles driving alone over hilly roads in [21], where an optimal controller that optimizes the fuel consumption of a single truck is proposed. In this paper, it was shown how, by using look-ahead control (LAC), a single vehicle is able to reduce its fuel consumption by up to 3.5%. The role of slopes becomes even more critical in the case of trucks driving in a platoon formation. The additional requirement of keeping a small inter-vehicular distance between vehicles collides indeed with the fact that trucks experience significantly different longitudinal forces (e.g., gravitational force depending on their mass and current road slope and air drag resistance depending on the distance from the previous vehicle). An experimental evidence of the problem is shown in [19], where a platoon is controlled by a distributed feedback control while driving over a public highway. In this paper, it is highlighted how the absence of topography information and coordination between vehicles can lead to a significant increase of the fuel consumption of the follower vehicles in the highway sectors with a particularly strong altitude variation.

There exist few works that address the inclusion of topography information in order to further improve the fuel-saving potential of vehicle platooning (see [22]–[24]). Alam *et al.* [22] and Németh and Gáspár [23] propose two control strategies that collect the fuel-optimal speed trajectories of each vehicle and combine them in order to obtain a single-speed trajectory for the whole platoon. In both works, however, the reduction of the aerodynamic drag due to the short inter-vehicular distance is not taken into account, and no guarantees on the optimality of the resulting speed trajectory for the platoon are provided. These two aspects are addressed in [24], where a centralized nonlinear model predictive controller is proposed for the coordination of the platooning vehicles. However, due to the complexity of the resulting model predictive control (MPC) problem, only a short prediction horizon can be implemented in real time. Such a short horizon does not allow one to capture the spatial dynamics of realistic topography profiles. Furthermore, in all these three works, the safety problem is not taken into account.

In this paper, we propose a novel cooperative LAC (CLAC) framework for fuel-efficient and safe heavy-duty vehicle platooning. The complex problem aimed at computing fuel-optimal, real-time, and safe control inputs for all the platooning vehicles is split into two manageable subproblems, and a control architecture is proposed to address them. The higher layer of such architecture, namely, the platoon coordinator, computes the fuel-optimal reference speed profile for the platoon. Such optimization relies on a dynamic programming (DP) formulation [25] that exploits preview information on the road topography and speed limits to

compute a speed trajectory that is safe and fuel optimal for the entire platoon. The reference speed profile is communicated to the lower layer, namely, the vehicle controller layer, that safely tracks it and computes the real-time inputs for each vehicle in the platoon. This layer is implemented by a distributed MPC formulation [26] that tracks the speed profile and the chosen gap policy while guarantying safety. Some early results of this study have been published in [27]. The main extensions of this paper are as follows. First, a theoretical framework for proving the safety of the platooning operations is proposed. It is proven that the proposed controller is able to avoid collisions in the case that no more than one of the platooning vehicles is driven manually. Second, we analyze an experimental platoon test to motivate the need for an LAC framework that coordinates the platooning vehicles. Finally, the proposed approach is evaluated by an extensive simulation study that compares its performance with standard control strategies. This analysis suggests the potential of the proposed controller to save up to 12% of fuel for follower vehicles compared with the use of standard platoon controllers from the literature.

The remainder of this paper is organized as follows. In Section II, we analyze the experimental results presented in [19] in order to obtain a good understanding of the role of the road gradient on truck platooning. In Section III, we present the vehicle and platoon models used in the control designs, whereas in Section IV, we introduce the control architecture. The platoon coordinator and the vehicle control layer are discussed in Sections V and VI, while their performance is studied in Sections VII–IX, by means of simulations. Finally, conclusions are stated in Section X.

II. MOTIVATING EXPERIMENT

In this section, we analyze the experimental results presented in [19] in order to obtain a good understanding of the impact of the road gradient on truck platoons and motivate the need for an LAC framework for fuel-efficient platooning.

In this experiment, a platoon of three similar heavy-duty vehicles (same powertrain and mass of 37.5, 38.4, and 39.5 tons, respectively) is driven over a 45-km highway stretch between the Swedish cities of Mariefred and Eskilstuna. The topography for this road is displayed in Fig. 1, where the red regions highlight the uphill and downhill sections for which the slope is too large for a nominal truck (whose parameters are displayed in Table I in Section VII) to maintain a constant speed of 22 m/s without braking or exceeding the engine power limit. For the considered road, the steep sections represent 23% of the total length. Overall, the results in [19] show that the follower vehicles, by platooning, reduce their fuel consumption by 4.1% and 6.5%, respectively. However, the authors highlight that the fuel efficiency drops significantly in the road sectors in which the altitude variation is larger. In this paper, we therefore focus on the behavior of the first two vehicles of the platoon while driving over the particularly hilly stretch highlighted in Fig. 1 as Sector A for which an increase of the fuel consumption of the second vehicle of 4% compared with the case of driving alone has been reported. The vehicles behavior is reported in Fig. 2. The first vehicle tracks a reference speed of 21.5 m/s using cruise control (CC)

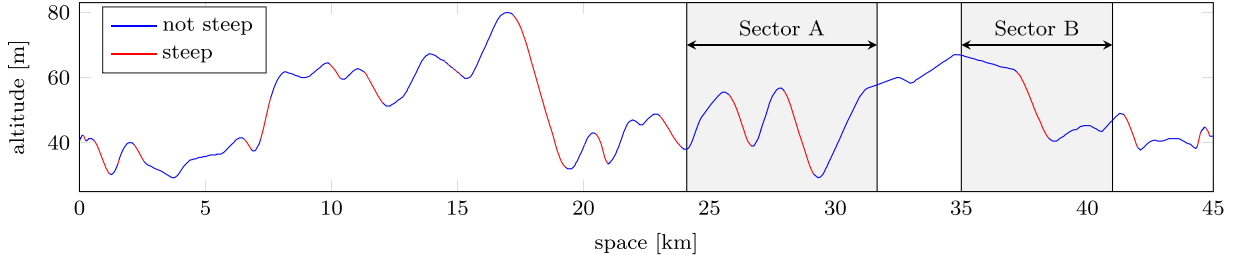


Fig. 1. Road topography for the 45-km highway stretch between the Swedish cities of Mariefred and Eskilstuna. The red regions highlight the uphill and downhill sections where the slope is too large for the vehicle considered (whose parameters are shown in Table I) to maintain a constant speed of 22 m/s without braking or exceeding the engine power limit.

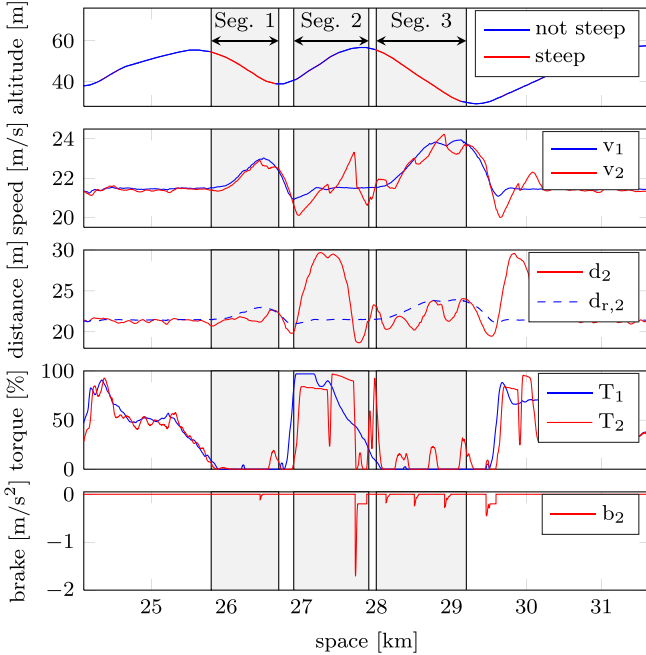


Fig. 2. Experiment results presented in [19] relative to the first two vehicles of a three vehicle platoon driving over Sector A highlighted in Fig. 1. First plot: the road topography. Second plot: the speed of the two vehicles. Third plot: the real and reference (according to a headway gap policy) between the vehicles. Fourth and fifth plots: the normalized engine torque for both vehicles and the normalized braking force for the second vehicle (the braking action of the first vehicle is not available), respectively. For additional details see [19].

and it switches to braking mode only when the speed limit of 23.6 m/s is reached. The second vehicle tracks a headway gap (a distance proportional to its speed) from the first vehicle and it switches to braking mode only when the headway gap reaches a certain threshold. Three critical segments highlighted in Fig. 2 are identified for which the sole use of feedback control shows its limitations.

- 1) *Segment 1:* Due to the steep downhill, the first vehicle is not able to maintain the reference speed, and therefore, it accelerates while coasting (i.e., traveling without injecting any fuel in the engine). The second vehicle, while trying to track the headway gap policy, follows the same behavior. However, due to the reduced experienced air resistance, during the downhill the second vehicle accelerates more than the first one and, when the critical headway gap is reached, it brakes. Coordination between the accelerations of the two vehicles has the potential of avoiding this undesired braking.

2) *Segment 2:* The headway gap deviates significantly from the reference one, due to a large relative speed at the beginning of the uphill segment and a change of gear during the segment. The second vehicle, in order to reduce the headway gap error, significantly increases its speed. Once the critical headway gap is reached, it strongly brakes. The prediction of the vehicles future behavior would allow the second vehicle to reduce the relative speed before reaching the reference headway gap and, therefore, to avoid the undesired braking.

3) *Segment 3:* Here, the second vehicle shows a more critical behavior compared with the downhill of Segment 1. In fact, during downhills, the vehicles' actuators work close to saturation (small throttling and small braking) which cannot be taken into account by a feedback controller. Therefore, in Segment 3, the control state of the second vehicle continues to switch between traction and braking modes. In addition, in order not to exceed the speed limit, both vehicles brake at the end of the downhill. The use of an MPC framework would allow one to predict correctly the vehicle behavior by taking topography information and actuator limits into account, and obtain therefore a smoother behavior of the vehicles.

The analysis of these experimental results provides a strong motivation for the development of a CLAC strategy for heavy-duty vehicle platooning based on a receding horizon framework where the road gradient and the preceding vehicles can be explicitly taken into account.

III. MODELING

In this section, we derive a high-level model of the vehicle suitable for fuel efficient and safe control. In particular, first, we introduce a model of the longitudinal dynamics of a single vehicle and a platoon with a particular focus on the components that play a significant role in the fuel consumption. Second, we present a simple fuel model that can be used to estimate the instantaneous fuel consumption.

A. Vehicle and Platoon Model

Using Newton's second law, the longitudinal dynamics of a single vehicle can be expressed by

$$\begin{aligned} m_i \dot{v}_i &= F_{e,i} + F_{b,i} + F_{g,i}(\alpha(s_i)) + F_{r,i} + F_{d,i}(v_i, d_i) \\ \dot{s}_i &= v_i \end{aligned} \quad (1)$$

where v_i and s_i denote the speed and the longitudinal position of vehicle i (we collect them in the state vector $x_i = [v_i \ s_i]^T$),

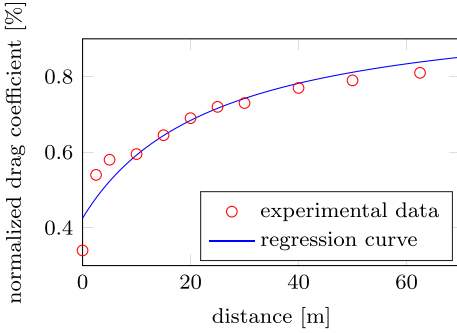


Fig. 3. Experimental data [29] and regression curve of the normalized drag coefficient experienced by a heavy-duty vehicle as function of the distance to the previous vehicle.

m_i is its mass, and $F_{e,i}$, $F_{b,i}$, $F_{g,i}$, $F_{r,i}$, and $F_{d,i}$ are the forces acting on the vehicle. More specifically, $F_{e,i}$ and $F_{b,i}$ are the control inputs and represent the forces generated by the powertrain and the braking system, respectively. The engine force $F_{e,i}$ will be characterized in Section III-B and the braking force $F_{b,i}$ is assumed to be limited by the road friction and therefore bounded by

$$-\eta_i \mu m_i g \leq F_{b,i} \leq 0 \quad (2)$$

where η_i , μ , and g denote the braking system efficiency, the (positive) road friction coefficient, and the gravitational acceleration, respectively. The forces $F_{g,i}$, $F_{r,i}$, and $F_{d,i}$ represent the state-dependent external forces acting on the vehicle. In particular, $F_{g,i}(\alpha(s_i))$ is the gravitational force, modeled as

$$F_{g,i}(\alpha(s_i)) = -m_i g \sin(\alpha(s_i)) \quad (3)$$

where $\alpha(s_i)$ is the road slope at position s_i . The force $F_{r,i}$ represents the rolling resistance, modeled as

$$F_{r,i} = -c_r m_i g \quad (4)$$

where c_r is the rolling coefficient. Finally, $F_{d,i}(v_i, d_i)$ is the aerodynamic drag, modeled as

$$F_{d,i}(v_i, d_i) = -\frac{1}{2} \rho A_v C_D(d_i) v_i^2 \quad (5)$$

where ρ is the air density, A_v is the cross-sectional area of the vehicle, and C_D is the air drag coefficient [28]. In order to take into account the influence of the inter-vehicular distance on the aerodynamic force that plays an essential role in platooning, the drag coefficient C_D is defined as a function of the distance to the previous vehicle d_i . This dependence is modeled by

$$C_D(d_i) = C_{D,0} \left(1 - \frac{C_{D,1}}{C_{D,2} + d_i} \right) \quad (6)$$

where the parameters $C_{D,1}$ and $C_{D,2}$ have been obtained by regressing the experimental data presented in [29]. The effect of the short inter-vehicular distance on the leading vehicle is neglected since it is smaller than one on the follower vehicles. The experimental data and the regression curve are displayed in Fig. 3.

Remark 1: In this paper, we have chosen to model the air drag coefficient on the basis of the experimental data presented

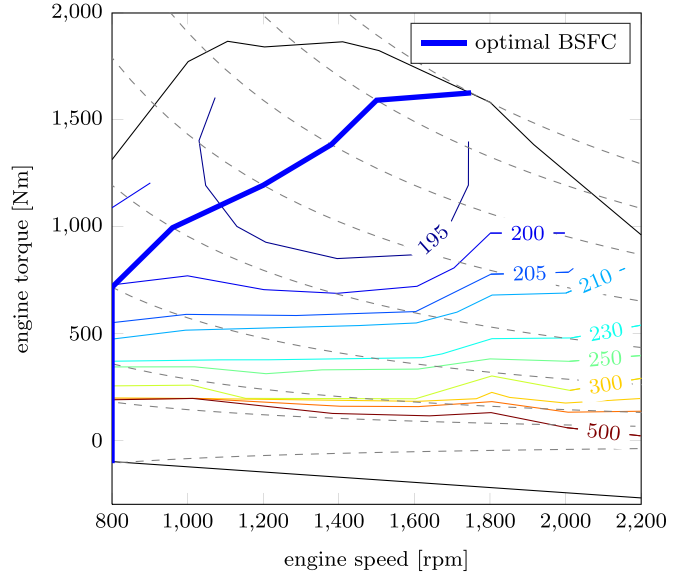


Fig. 4. BSFC map for a 400-hp engine regenerated from [31]. The plot shows the BSFC expressed in g/kWh as function of the engine speed and torque. Dotted lines: equal power curves. Blue thick line: the collection of the fuel-optimal operation points per various generated powers.

in [29] relative to the second vehicle of a two bus platoon driving at 80 km/h. In the literature, reports on air drag coefficient or fuel consumption measures based on both real experiments [8], [10] and fluid dynamics computations [30] are presented. They show a reduction of the air drag coefficient for short inter-vehicular distances. How the reduction relates to the inter-vehicular distance varies. This variability has been attributed to the weather condition (e.g., temperature, humidity, or wind) and the shape of the vehicles.

The model of a platoon of N_v vehicles is given by the combination of (1) for $i = 1, \dots, N_v$ and the distance definition

$$d_i = \begin{cases} \infty, & \text{if } i = 1 \\ s_{i-1} - s_i - l_{i-1}, & \text{if } i \geq 2 \end{cases} \quad (7)$$

where l_i denotes the length of vehicle i .

B. Fuel Model

The powertrain is a complex system composed of engine, clutch, gearbox, and final gear that allows one to transform the fuel's energy into longitudinal force. In this section, we derive a simple model of the powertrain that captures the intrinsic relation between consumed fuel and generated traction force. In the model derivation, we ignore transmission energy losses and the rotational inertia of the powertrain components because they are assumed to be negligible when compared with the vehicle mass.

Engine performance is typically described by the brake-specific fuel consumption (BSFC), which defines the ratio between consumed fuel and generated energy for various operation points (i.e., engine speed and generated torque). In Fig. 4, we show the BSFC map for a truck engine of 400 hp [31], where the dotted lines represent the collection of operation points with equal generated power. This map can be easily converted into one that defines the fuel flow δ_i as

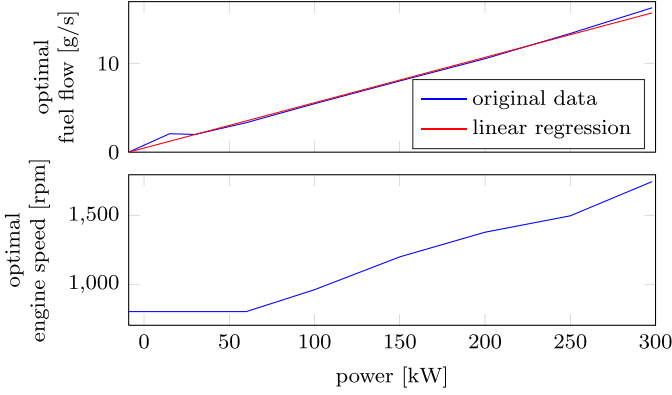


Fig. 5. Plots of the optimal fuel flow and engine speed as function of the generated power. In the first plot, we also display the fuel model expressed in (10) obtained by the regression of the raw data.

function of the engine speed ω_i and the generated engine power P_i , i.e., $\delta_i = \phi_i(\omega_i, P_i)$. By assumption, the engine power P_i , passing through the clutch, the gearbox, and the final gear, is completely transferred to the wheels. The rotational speed, instead, changes between the transmission components and is finally transformed into longitudinal speed by the wheels. Ultimately, under the assumption of no longitudinal slip, the vehicle speed v_i can be defined as $v_i = k_i g_i \omega_i$, where k_i is a constant gain and g_i is the gear ratio of the gearbox. Therefore, the fuel flow can be expressed as a function of the speed v_i , the traction force $F_{e,i}$, and the gear ratio g_i as

$$\delta_i = \phi_i \left(\frac{v_i}{k_i g_i}, F_{e,i} v_i \right). \quad (8)$$

In order to be efficiently used in the control design, the fuel model is further simplified by removing the dependence of the fuel flow δ_i on the gear ratio g_i through the introduction of the following additional assumption.

- 1) The gear ratio can be changed continuously on a unlimited span.
- 2) The gear management system chooses the most efficient gear ratio.

Hence, we redefine the fuel model as

$$\delta_i = \min_{\omega_i} \phi_i(\omega_i, F_{e,i} v_i) = \phi_{\text{opt},i}(F_{e,i} v_i). \quad (9)$$

The resulting curve $\phi_{\text{opt},i}(\cdot)$ is depicted in Fig. 5 and is linearly regressed in order to obtain the fuel model used in the controller design, defined by

$$\delta_i = p_{1,i} F_{e,i} v_i + p_{0,i}. \quad (10)$$

From this analysis, we can also obtain the bounds on the generated power that are independent of the engine speed and the gear ratio

$$P_{\min,i} \leq F_{e,i} v_i \leq P_{\max,i}. \quad (11)$$

In Fig. 5, the two fuel models in (9) and (10), and the correspondent optimal engine speed are displayed. We note that the approximation error is negligible.

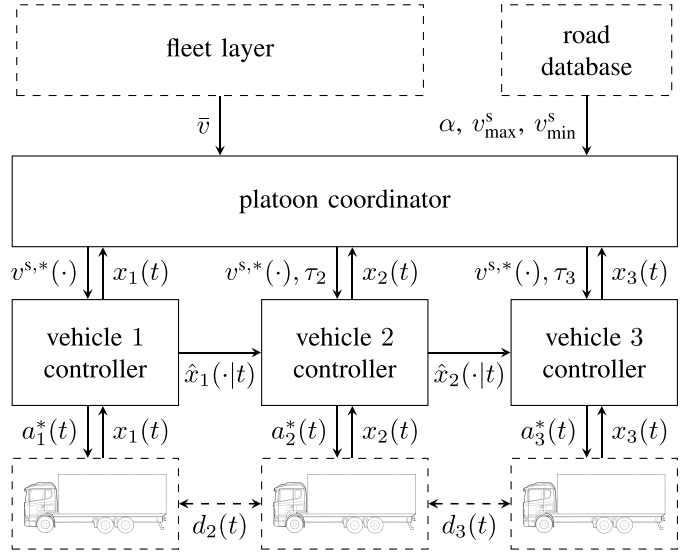


Fig. 6. System architecture for look-ahead heavy-duty vehicle platooning.

IV. PLATOON CONTROLLER ARCHITECTURE

In this section, we present the control architecture aimed at splitting the complex problem of computing real-time, fuel-efficient, and safe control inputs for all vehicles into two simpler layers. The system architecture is displayed in Fig. 6. Within this architecture, the platoon coordinator supervises the platoon behavior exploiting road information and average speed requirements communicated by the fleet layer [28]. The vehicle control layer, instead, executes the reference speed profile generated by the platoon coordinator for the individual vehicles.

More in detail, the platoon coordinator layer exploits available information on the topography of the planned route to find a fuel-optimal speed profile for the entire platoon, while satisfying an average speed requirement provided by the fleet layer. Hereby, in order to capture the dynamics induced by the road topography, it considers a horizon of several kilometers and takes the constraints of all vehicles in the platoon into account. As a result, it can be guaranteed that every vehicle in the platoon is able to track the required speed profile. A single-speed trajectory is computed by the platoon coordinator, representing the speed of the platoon. However, when this speed profile is specified as a function of space (i.e., position on the road) and the inter-vehicular spacing is chosen according to a pure time gap, every individual vehicle in the platoon can track this single-speed profile. It is remarked that this layer operates in a receding horizon fashion, providing an updated speed profile roughly every 10 s or when the recalculation is needed due to a strong deviation from the original speed profile. Finally, as this layer is not safety critical and not related to a specific vehicle, it can be implemented in any of the platooning vehicles or even in an off-board roadside unit. In Section V, we present a DP approach to formulate and solve the stated problem.

The vehicle controller is responsible for the real-time control of each vehicle in the platoon and is aimed at tracking the desired speed profile as resulting from the platoon coordinator.

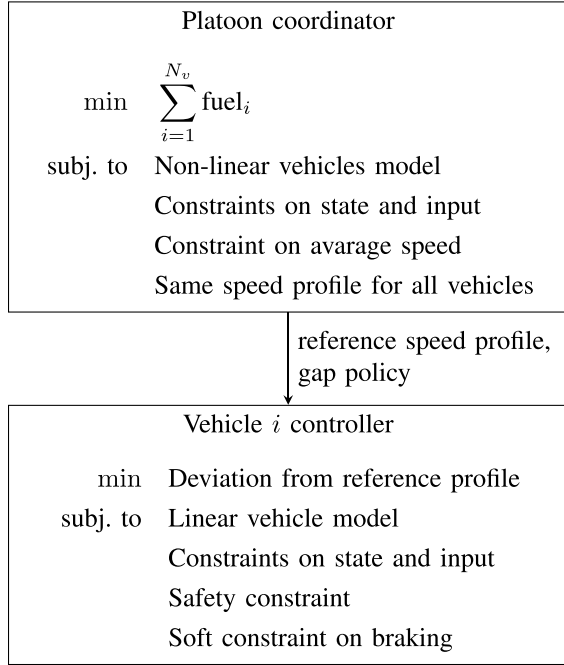


Fig. 7. Optimal control problems formulations for the platoon coordinator and vehicle controllers. In Section V, the problem formulation of the platoon coordinator is simplified by relaxing the constraint on average speed in order to decrease the problem complexity.

It also exploits the communication between the vehicles of their trajectories to ensure the proper spacing. This layer guarantees the safety of platooning operations by ensuring that collisions between trucks will not occur. Because of the safety-critical aspect, this layer is implemented in a distributed fashion in each vehicle of the platoon. In Section VI, a distributed MPC approach for this problem is discussed.

Fig. 7 shows how the optimization problems in the platoon coordinator and the vehicle controllers interact, and their mathematical structure. Note how the platoon coordinator, in order to have a good prediction of the consumed fuel over the horizon, uses an accurate nonlinear model of each vehicle, while the vehicle control layer, in order to enable the fast computation necessary for the real-time control of the vehicle, uses a linear vehicle model.

V. PLATOON COORDINATOR

The platoon coordinator is the higher layer of the platoon control architecture. It takes as inputs the average speed requirement \bar{v} from the fleet layer and the current vehicle state $x_i(t)$ from the vehicle controller. By exploiting the available information on the planned route (i.e., slope data α and speed limits v_{\min}^s and v_{\max}^s), it generates a unique feasible and fuel-optimal speed profile $v^{s,*}(\cdot)$ defined over space for all the vehicles within the platoon [i.e., $v_i^{s,*}(z) = v^{s,*}(z)$ for $i = 1, \dots, N_v$, where z is the spacial variable]. Furthermore, it specifies the time gaps τ_i , defined as the time intervals between two consecutive vehicles passing through the same point [32], that is

$$s_i(t) = s_{i-1}(t - \tau_i). \quad (12)$$

Note that this spacing policy is consistent with the requirement that all vehicles have to follow the same speed profile over space. This can be easily shown by computing the time derivative of the left-hand side of (12), leading to

$$\frac{ds_i(t)}{dt} = v_i(t) = v_i^s(s_i(t)) \quad (13)$$

and the right-hand side of (12), leading to

$$\begin{aligned} \frac{ds_{i-1}(t - \tau_i)}{dt} &= v_{i-1}(t - \tau_i) \\ &= v_{i-1}^s(s_{i-1}(t - \tau_i)) = v_{i-1}^s(s_i(t)) \end{aligned} \quad (14)$$

where $v_i^s(s)$ denotes the speed of vehicle i at space s . By combining (12)–(14), we obtain $v_i^s(s) = v_{i-1}^s(s)$. The time gap τ_i is chosen as a tradeoff between fuel efficiency and safety. A too large time gap, in fact, would not fully exploit the potential of platooning, while a too small time gap would lead to the frequent activation of the safety constraints implemented in the vehicle control layer and, therefore, to undesired braking.

Remark 2: We use time gap to define a desired inter-vehicular spacing policy. This differs from the time-delay effects due to limitations in the (wireless) communication between vehicles in a platoon (see [33], [34]), which will be accounted for in the distributed vehicle control layer.

The coordinator layer is implemented using a DP framework that runs in closed loop. The parameters that characterize the DP problem are the discretization space Δs_{DP} , the horizon length H_{DP} , and the refresh frequency f_{DP} . We also define the horizon space length as $S_{DP} = H_{DP}\Delta s_{DP}$.

In Sections V-A–V-D, we introduce all the components of the DP formulation, i.e., the vehicle model, the constraints on the input and states, and finally, the cost function.

A. Platoon Model

The platoon coordinator layer uses a discretized version of the vehicle model (1), where the discretization is carried out in the spacial domain using the implicit Euler approximation. The discretized vehicle model is

$$\begin{aligned} v_i^s(z_k) \frac{v_i^s(z_k) - v_i^s(z_{k-1})}{\Delta s_{DP}} &= F_{e,i}^s(z_k) + F_{b,i}^s(z_k) \\ &\quad - m_i g [\sin \alpha(z_k) + c_r] \\ &\quad - \frac{1}{2} \rho A_v C_D (d_i^s(z_k)) (v_i^s(z_k))^2 \end{aligned} \quad (15a)$$

$$v_i^s(z_k) \frac{t_i^s(z_k) - t_i^s(z_{k-1})}{\Delta s_{DP}} = 1 \quad (15b)$$

where z_k is the discretized spacial variable, $v_i^s(z_k)$, $F_{e,i}^s(z_k)$, $F_{b,i}^s(z_k)$, and $d_i^s(z_k)$ are the speed, the engine and braking forces, and the distance to the preceding vehicle, respectively, all expressed as function of space.

The advantage of using the space discretization is that, by relaxing the average speed requirement, there is no constraint depending on time. The relaxation is done by removing the average speed constraint and introducing instead the traveled time in the cost function as described in Section V-C. This relaxation allows one to ignore the time dynamics of the

vehicles and therefore significantly reduce the computational complexity.

A drawback of the space discretization is that the distance definition (7) cannot be expressed in the spacial domain. Instead, the following approximated expression, as function of the current vehicle speed $v_i^s(z_k)$, is used:

$$d_i^s(z_k) = v_i^s(z_k)\tau_i - l_{i-1}. \quad (16)$$

In the DP formulation, we refer to (15a) as $v_i^s(z_{k-1}) = f_{v,i}^s(v_i^s(z_k), u_i^s(z_k))$, where $u_i^s(z_k)$ is the input vector defined as $u_i^s(z_k) = [F_{e,i}^s(z_k) \ F_{b,i}^s(z_k)]^T$.

B. Model Constraints

The platoon model is constrained by bounds on the input and the speed.

1) *Input Constraints*: According to (2) and (11), the engine and braking forces are bounded by the following constraints:

$$\begin{aligned} P_{\min,i}/v_i^s(z_k) &\leq F_{e,i}^s(z_k) \leq P_{\max,i}/v_i^s(z_k) \\ -\eta_i \mu m_i g &\leq F_{b,i}^s(z_k) \leq 0. \end{aligned} \quad (17)$$

In the DP formulation, we refer to these constraints as $u_i^s(z_k) \in \mathcal{U}_i^s(z_k, v_i^s)$.

2) *State Constraints*: In order to take into account the road speed limits, the speed is bounded by

$$v_{\min}(z_k) \leq v_i^s(z_k) \leq v_{\max}(z_k). \quad (18)$$

We refer to this constraint as $v_i^s(z_k) \in \mathcal{V}^s(z_k)$.

Moreover, in order to require all the vehicle to follow the same speed profile, the constraint:

$$v_i^s(z_k) = v^s(z_k), \quad i = 1, \dots, N_v \quad (19)$$

is introduced. Here, we emphasize that the practical effect of the last constraint is to reduce the search space of the DP algorithm to one dimension enabling fast computations.

C. Cost Function

The objective of the platoon coordinator is to define the optimal speed profile that minimizes the fuel consumption of the whole platoon, while maintaining a certain average speed. This is done by defining the cost function as the weighted sum of two terms: a first term $J_f(v^s(z_J), u_I^s(z_J))$ with $z_J = [z_k, \dots, z_{k+H_{DP}-1}]$ and $I = [1, \dots, N_v]$ representing the amount of fuel consumed by the platoon and a second term $J_t(v^s(z_J))$ representing the traveled time over the horizon, that is

$$J_{DP}(v^s(z_J), u_I^s(z_J)) = J_f(v^s(z_J), u_I^s(z_J)) + \beta J_t(v^s(z_J)) \quad (20)$$

where β represents a tradeoff weight.¹ The term $J_f(v^s(z_J), u_I^s(z_J))$ is computed by using the fuel model (10),

¹Instead of the constraint on the average speed of Fig. 7, the parameter β is tuned to give the desired average travel time.

taking also into account a final term representing the kinematic energy of the platoon at the end of the horizon

$$\begin{aligned} J_f(v^s(z_J), u_I^s(z_J)) &= \sum_{i=1}^{N_v} \sum_{j=k}^{k+H_{DP}-1} \Delta s_{DP} \left(p_{1,i} F_{e,i}^s(z_j) + \frac{p_{0,i}}{v^s(z_j)} \right) \\ &\quad - \sum_{i=1}^{N_v} p_{1,i} \frac{m_i (v^s(z_{h+H_{DP}-1}))^2}{2}. \end{aligned}$$

The term $J_t(v^s(z_J))$ is obtained by using the time model (15b)

$$J_t(v^s(z_J)) = \sum_{j=k}^{k+H_{DP}-1} \frac{\Delta s_{DP}}{v^s(z_j)}.$$

D. Dynamic Programming Formulation

We now have all the elements to formulate the DP problem solved in the platoon coordinator

$$\min_{u_I^s(z_J)} J_{DP}(v^s(z_J), u_I^s(z_J)) \quad (21a)$$

$$\text{s.t. } v_i^s(z_{j-1}) = f_{v,i}^s(v_i^s(z_j), u_i^s(z_j)) \quad (21b)$$

$$u_i^s(z_j) \in \mathcal{U}_i^s(z_j, v_i^s) \quad (21c)$$

$$v_i^s(z_j) = v^s(z_j) \in \mathcal{V}^s(z_j) \quad (21d)$$

$$z_k = s_1(t) \quad (21e)$$

$$v^s(z_k) = v_1(t) \quad (21f)$$

for $j = k, \dots, k + H_{DP} - 1$, where (21e) and (21f) represent the initial conditions for each iteration.

VI. VEHICLE CONTROLLER

This section focuses on the distributed MPC-based controllers running in the vehicle control layer. Each vehicle controller runs locally. Vehicle i receives the optimal speed profile $v^{s,*}(\cdot)$ and the time gap τ_i from the platoon coordinator and obtains state information from the preceding vehicle. By tracking the optimal speed profile and the gap policy requirement, while satisfying a safety constraint, it generates the optimal state and input trajectories, respectively, $x_i^*(\cdot|t)$ and $a_i^*(\cdot|t)$, and the desired instantaneous acceleration $a_i^*(t)$ for the vehicle engine and braking management systems. The parameters that characterize the MPC formulation are the discretization time Δt_{MPC} , the horizon steps number H_{MPC} , the refresh frequency f_{MPC} , and the length of the horizon defined as $T_{MPC} = H_{MPC} \Delta t_{MPC}$.

In Sections VI-A–VI-E, we introduce all the components of the MPC formulation, i.e., the vehicle model, the constraints on the input and state, the safety constraint and, finally, the cost function.

A. Vehicle Model

In the MPC formulation the vehicle is described by

$$x_i(t_{j+1}|t_k) = Ax_i(t_j|t_k) + Ba_i(t_j|t_k) \quad (22)$$

where

$$A \triangleq \begin{bmatrix} 1 & 0 \\ \Delta t_{\text{MPC}} & 1 \end{bmatrix}, \quad B \triangleq \begin{bmatrix} \Delta t_{\text{MPC}} \\ 0 \end{bmatrix}.$$

The variables $x_i(t_j|t_k) = [v_i(t_j|t_k) \ s_i(t_j|t_k)]^T$ and $a_i(t_j|t_k)$ denote the predicted state (speed and position) and control input (desired acceleration) trajectories of vehicle i associated with the update time t_k . We also introduce three additional trajectories associated with each update time t_k that will be used later in the MPC formulation:

- 1) the optimal state trajectory $x_i^*(t_j|t_k)$;
- 2) the state reference trajectory $\bar{x}_i(t_j|t_k)$;
- 3) the assumed state trajectory $\hat{x}_i(t_j|t_k)$.

The value of j is defined as $j = k, \dots, k + H_{\text{MPC}} - 1$ and the corresponding input control trajectories defined likewise. While the predicted and optimal trajectories are functions of the optimization variable, the reference and assumed trajectories are precomputed. More precisely the reference trajectories $\bar{x}_i(t_j|t_k) = [\bar{v}_i(t_j|t_k) \ \bar{s}_i(t_j|t_k)]^T$ and $\bar{a}_i(t_j|t_k)$ are computed from the reference trajectory $v^{s,*}(\cdot)$ and the current position $s(t_k)$ of the vehicle. In particular, $\bar{s}_i(t_j|t_k)$ is defined recursively as

$$\bar{s}_i(t_j|t_k) = \begin{cases} s_i(t_j), & j = k \\ \bar{s}_i(t_{j-1}|t_k) + \Delta t_{\text{MPC}} v^{s,*}(\bar{s}_i(t_{j-1}|t_k)), & j > k \end{cases}$$

while $\bar{v}_i(t_j|t_k)$ is defined as

$$\bar{v}_i(t_j|t_k) = v^{s,*}(\bar{s}_i(t_j|t_k)).$$

The control input reference trajectory $\bar{a}_i(t_j|t_k)$ is defined as finite differences of $\bar{v}_i(t_j|t_k)$, that is

$$\bar{a}_i(t_j|t_k) = (\bar{v}_i(t_{j+1}|t_k) - \bar{v}_i(t_j|t_k)) / \Delta t_{\text{MPC}}. \quad (23)$$

The assumed state and control input trajectories are computed from the optimal and real trajectories of the vehicle as

$$\hat{x}_i(t_j|t_k) = \begin{cases} x_i(t_j), & j < k \\ x_i^*(t_{k-1}|t_k), & k \leq j < k + H_{\text{MPC}} \end{cases} \quad (24)$$

and $\hat{a}_i(t_j|t_k)$ likewise. Each vehicle communicates the assumed trajectory $\hat{x}_i(t_j|t_k)$ to the follower one. In this case, the use of the optimal trajectory computed the previous step reflects the assumption of a maximum communication delay of Δt_{MPC} .

B. Input and Model Constraints

In order to take the bounds on the braking force (2) and the engine power (11) into account, as done in the platoon coordinator layer, the control input a_i is bounded by the following nonlinear constraint:

$$-\eta_i \mu g + \frac{F_{\text{ext}}(x_i, \hat{s}_{i-1})}{m_i} \leq a_i \leq \frac{P_{i,\max}}{m_i v_i} + \frac{F_{\text{ext}}(x_i, \hat{s}_{i-1})}{m_i} \quad (25)$$

where $F_{\text{ext}}(x_i, \hat{s}_{i-1})$ denotes the summation of the external forces acting on the vehicle and is defined as

$$F_{\text{ext}}(x_i, \hat{s}_{i-1}) = -m_i g (\sin(\alpha(s_i)) + c_r) - \frac{1}{2} \rho A_v C_D (\hat{s}_{i-1} - s_i - l_i) v_i^2. \quad (26)$$

The control input is additionally bounded by a soft constraint in order to allow braking only if necessary, i.e., when the safety constraint (see Section VI-C) is activated or the braking is required by the platoon coordinator. This is formulated as follows:

$$a_i + \epsilon_i \geq \min(a_{c,i}, \bar{a}_i), \quad \epsilon_i \geq 0 \quad (27)$$

where ϵ_i is the softening variable, \bar{a}_i is the input reference trajectory defined in (23), and $a_{c,i}$ is the coasting acceleration (i.e., no braking and fuel injection) defined as

$$a_{c,i} = \frac{P_{i,\min}}{m_i v_i} + \frac{F_{\text{ext}}(x_i, \hat{s}_{i-1})}{m_i}. \quad (28)$$

In the MPC formulation, we refer to the constraint (25) and (26) as $a_i(t_j|t_k) \in \mathcal{A}_i(x_i(t_j|t_k))$ and to the soft constraint (27) and (28) as $a_i(t_j|t_k) + \epsilon_i(t_j|t_k) \in \mathcal{A}_{\epsilon,i}(x_i(t_j|t_k))$.

The speed is bounded according to the constraint (18) as

$$v_{\min}(s_i(t_j|t_k)) \leq v_i(t_j|t_k) \leq v_{\max}(s_i(t_j|t_k)).$$

In the MPC formulation, we refer to this constraint as $v_i(t_j|t_k) \in \mathcal{V}(s_i(t_j|t_k))$.

C. Safety Constraint

The platoon is intended to operate on public highways where other vehicles are present. The designed controller therefore should be able to cope with cases where the platoon behavior deviates from the predicted one because of internal disturbances (e.g., gearshifts) or external events (e.g., dense traffic or a vehicle cutting into the platoon). In this section, we focus on the safety problem, leaving to further work the study of how such events should be handled (i.e., autonomously or by switching to manual driving).

The platoon is considered safe if, whatever a vehicle in the platoon does, there exists an input for all the follower vehicles such that a collision can be avoided (see also [35]). The safety of the platoon is guaranteed by ensuring that the state of each vehicle lies within a safety set and it is first studied by considering two adjacent vehicles and later extended to the entire platoon. Consider the following continuous-time vehicle dynamics:

$$\dot{\tilde{x}}_i = \begin{bmatrix} \dot{\tilde{v}}_i \\ \dot{\tilde{s}}_i \end{bmatrix} = f(\tilde{x}_i, \tilde{a}_i) = \begin{bmatrix} \tilde{a}_i \\ \tilde{v}_i \end{bmatrix} \quad (29)$$

where \tilde{v}_i , \tilde{s}_i , and \tilde{a}_i are the speed, position, and acceleration of vehicle i , respectively.

Let now focus on the dynamics of two adjacent vehicles described by

$$\begin{bmatrix} \dot{\tilde{x}}_{i-1} \\ \dot{\tilde{x}}_i \end{bmatrix} = F(\tilde{x}_{i-1}, \tilde{x}_i, \tilde{a}_{i-1}, \tilde{a}_i) = \begin{bmatrix} f(\tilde{x}_{i-1}, \tilde{a}_{i-1}) \\ f(\tilde{x}_i, \tilde{a}_i) \end{bmatrix} \quad (30)$$

where the acceleration of the current vehicle \tilde{a}_i is the control input, while the acceleration of the preceding vehicle \tilde{a}_{i-1} is the exogenous input that can be regarded as a disturbance. We also introduce the admissible set $\tilde{\mathcal{X}} = \{[\tilde{x}_{i-1}^T \ \tilde{x}_i^T]^T : \tilde{v}_{i-1} \geq 0, \tilde{v}_i \geq 0, \tilde{s}_{i-1} - \tilde{s}_i \geq l_{i-1}\}$ as the set of all admissible states, where l_i denotes the length of vehicle i . In order to obtain a closed form of the safety set,

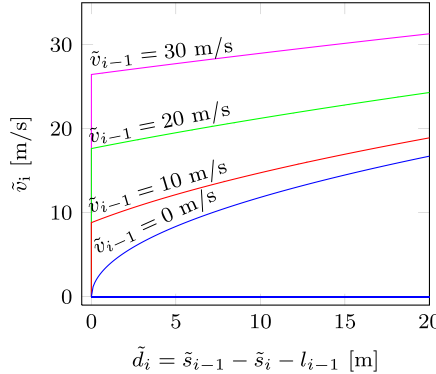


Fig. 8. Projection of the boundary $\partial\mathcal{S}_i$ of the safety set $\mathcal{S}_i \subseteq \tilde{\mathcal{X}}$ on the $(\tilde{d}_i, \tilde{v}_i)$ plane for $\tilde{v}_{i-1} = 0, 10, 20$, and 30 m/s. The variable \tilde{d}_i denotes the distance between the two adjacent vehicles (i.e., $\tilde{d}_i = \tilde{s}_{i-1} - \tilde{s}_i - l_{i-1}$).

the following conservative approximations of the exogenous and control inputs are introduced:

$$\tilde{a}_{i-1} \in \mathcal{A}^p(\tilde{x}_{i-1}) = \begin{cases} [\underline{a}_{\min,i-1}, \bar{a}_{\max,i-1}], & \text{if } \tilde{v}_{i-1} > 0 \\ [0, \bar{a}_{\max,i-1}], & \text{if } \tilde{v}_{i-1} = 0 \end{cases} \quad (31a)$$

$$\tilde{a}_i \in \mathcal{A}^f(\tilde{x}_i) = \begin{cases} [\bar{a}_{\min,i}, \underline{a}_{\max,i}], & \text{if } \tilde{v}_i > 0 \\ [0, \underline{a}_{\max,i}], & \text{if } \tilde{v}_i = 0 \end{cases} \quad (31b)$$

where $\underline{a}_{\min,i}$, $\bar{a}_{\min,i}$, $\underline{a}_{\max,i}$, and $\bar{a}_{\max,i}$ are the lower and upper bounds on the minimum and maximum possible accelerations of vehicle i , respectively. Such bounds are computed under reasonable assumptions on the vehicles and road properties, i.e., the vehicles' speed is limited ($0 \leq \tilde{v}_i \leq v_{\max}$) and the road slope α is bounded ($|\alpha| \leq \alpha_{\max}$). For example, the bounds $\underline{a}_{\min,i}$ and $\bar{a}_{\min,i}$ represent the minimum braking acceleration in the best and worst case environmental conditions. They can be computed as

$$\begin{aligned} \underline{a}_{\min,i} &= \min_{0 \leq v \leq v_{\max}, |\alpha| \leq \alpha_{\max}, d \geq 0} a_{\min,i}(v, \alpha, d) \\ \bar{a}_{\min,i} &= \max_{0 \leq v \leq v_{\max}, |\alpha| \leq \alpha_{\max}, d \geq 0} a_{\min,i}(v, \alpha, d) \end{aligned}$$

where $a_{\min,i}$ is derived from (1) and (2) and is defined as

$$a_{\min,i}(v, \alpha, d) = -\eta_i \mu g - g \sin(\alpha) - c_r g - \frac{\rho A_v C_D(d)v^2}{2m_i}.$$

Note that, due to the definition of the bounds and because of the dominance of the $-\eta_i \mu g$ term in the definition of $a_{\min,i}$, the following inequalities hold:

$$\underline{a}_{\min,i} \leq \bar{a}_{\min,i} \leq 0 \quad (33a)$$

$$\underline{a}_{\max,i} \leq \bar{a}_{\max,i}. \quad (33b)$$

In order to guarantee the safety of the subsystem (30), we should guarantee that the state $[\tilde{x}_{i-1}^T \tilde{x}_i^T]^T$ always lies in a safety set \mathcal{S}_i included in $\tilde{\mathcal{X}}$, for any admissible trajectory of the preceding vehicle. We now define the safety set $\mathcal{S}_i \subseteq \tilde{\mathcal{X}}$, displayed in Fig. 8, as

$$\mathcal{S}_i = \{[\tilde{x}_{i-1}^T \tilde{x}_i^T]^T : g_j(\tilde{x}_{i-1}, \tilde{x}_i) \geq 0, j = 1, \dots, 4\} \quad (34)$$

where

$$\begin{aligned} g_1(\tilde{x}_{i-1}, \tilde{x}_i) &= \tilde{s}_{i-1} - \tilde{s}_i - l_{i-1} - \frac{\tilde{v}_{i-1}^2}{2\underline{a}_{\min,i-1}} + \frac{\tilde{v}_i^2}{2\bar{a}_{\min,i}} \\ g_2(\tilde{x}_{i-1}, \tilde{x}_i) &= \tilde{s}_{i-1} - \tilde{s}_i - l_{i-1} \\ g_3(\tilde{x}_{i-1}, \tilde{x}_i) &= \tilde{v}_{i-1} \\ g_4(\tilde{x}_{i-1}, \tilde{x}_i) &= \tilde{v}_i \end{aligned} \quad (35)$$

and we state the following result.

Lemma 1: Given the dynamical system (30) and the constraints (31a) and (31b) on the exogenous and control inputs, respectively, there exists a control law $\tilde{a}_i = \phi([\tilde{x}_{i-1}^T \tilde{x}_i^T]^T) \in \mathcal{A}^f(\tilde{x}_i)$ such that for all $[\tilde{x}_{i-1}^T(t_0) \tilde{x}_i^T(t_0)]^T \in \mathcal{S}_i$ and $\tilde{a}_{i-1} \in \mathcal{A}^p(\tilde{x}_{i-1})$, the condition $[\tilde{x}_{i-1}^T(t) \tilde{x}_i^T(t)]^T \in \mathcal{S}_i$ holds for all $t \geq t_0$. In other words, \mathcal{S}_i is a robust controlled invariant set [36].

Proof: By using Nagumo's theorem for robust controlled invariant sets [36], the lemma can be proven by showing that for all $[\tilde{x}_{i-1}^T \tilde{x}_i^T]^T \in \partial\mathcal{S}_i$ (defined as the boundary of \mathcal{S}_i), there exists an $\tilde{a}_i \in \mathcal{A}^f$ such that, for all $\tilde{a}_{i-1} \in \mathcal{A}^p$, the relation

$$\nabla g_j(\tilde{x}_{i-1}, \tilde{x}_i)^T F(\tilde{x}_i, \tilde{x}_{i-1}, \tilde{a}_{i-1}, \tilde{a}_i) \geq 0 \quad (36)$$

holds for all j such that $g_j(\tilde{x}_{i-1}, \tilde{x}_i) = 0$. Because of the structure of the problem, the control input \tilde{a}_i is chosen as maximum braking, that is

$$\tilde{a}_i = \begin{cases} \bar{a}_{\min,i}, & \text{if } \tilde{v}_i > 0 \\ 0, & \text{if } \tilde{v}_i = 0 \end{cases} \quad (37)$$

for any $[\tilde{x}_{i-1}^T \tilde{x}_i^T]^T \in \partial\mathcal{S}_i$ and $\tilde{a}_{i-1} \in \mathcal{A}^p(\tilde{x}_{i-1})$. We organize the proof by considering $[\tilde{x}_{i-1}^T \tilde{x}_i^T]^T \in \partial\mathcal{S}_i$ defined by the activation of each $g_j(\tilde{x}_{i-1}, \tilde{x}_i) \geq 0$.

- 1) For $[\tilde{x}_{i-1}^T \tilde{x}_i^T]^T$ such that $g_1(\tilde{x}_{i-1}, \tilde{x}_i) = 0$, and $g_j(\tilde{x}_{i-1}, \tilde{x}_i) \geq 0$, for $j \in \{2, 3, 4\}$

$$\begin{aligned} \nabla g_1(\tilde{x}_{i-1}, \tilde{x}_i)^T F(\tilde{x}_{i-1}, \tilde{x}_i, \tilde{a}_{i-1}, \tilde{a}_i) &= \left(1 - \frac{\tilde{a}_{i-1}}{\underline{a}_{\min,i-1}}\right)\tilde{v}_{i-1} - \left(1 - \frac{\tilde{a}_i}{\bar{a}_{\min,i}}\right)\tilde{v}_i \\ &= \left(1 - \frac{\tilde{a}_{i-1}}{\underline{a}_{\min,i-1}}\right)\tilde{v}_{i-1} \geq 0 \end{aligned}$$

where the equality and the inequality hold because of the definition of \tilde{a}_i in (37) and $g_3(\tilde{x}_{i-1}, \tilde{x}_i) \geq 0$.

- 2) For $[\tilde{x}_{i-1}^T \tilde{x}_i^T]^T$ such that $g_2(\tilde{x}_{i-1}, \tilde{x}_i) = 0$, and $g_j(\tilde{x}_{i-1}, \tilde{x}_i) \geq 0$, for $j \in \{1, 3, 4\}$

$$\nabla g_2(\tilde{x}_{i-1}, \tilde{x}_i)^T F(\tilde{x}_{i-1}, \tilde{x}_i, \tilde{a}_{i-1}, \tilde{a}_i) = \tilde{v}_{i-1} - \tilde{v}_i \geq 0$$

where the inequality holds by noticing that the combination of $g_1(\tilde{x}_{i-1}, \tilde{x}_i) \geq 0$ and $g_2(\tilde{x}_{i-1}, \tilde{x}_i) = 0$, and the relation (33a) gives $\tilde{v}_{i-1} \geq (\underline{a}_{\min,i}/\bar{a}_{\min,i})\tilde{v}_i$.

- 3) For $[\tilde{x}_{i-1}^T \tilde{x}_i^T]^T$ such that $g_3(\tilde{x}_{i-1}, \tilde{x}_i) = 0$, and $g_j(\tilde{x}_{i-1}, \tilde{x}_i) \geq 0$, for $j \in \{1, 2, 4\}$

$$\nabla g_3(\tilde{x}_{i-1}, \tilde{x}_i)^T F(\tilde{x}_{i-1}, \tilde{x}_i, \tilde{a}_{i-1}, \tilde{a}_i) = \tilde{a}_{i-1} \geq 0$$

where the inequality holds because of (31a). The same can be verified in a similar way for $[\tilde{x}_{i-1}^T \tilde{x}_i^T]^T$ such that $g_4(\tilde{x}_{i-1}, \tilde{x}_i) = 0$ and $g_j(\tilde{x}_{i-1}, \tilde{x}_i) \geq 0$ for $j \in \{1, 2, 3\}$. \square

The choice of the safety set guarantees that the follower vehicle can react to the emergency braking maneuver of its predecessor, such that both vehicles come to a standstill without colliding. We now extend the result in Lemma 1 to the safety of the whole platoon. More precisely, we prove that whatever a vehicle does, there exists an input for all the follower vehicles, such that collision can be avoided. This is formalized by the following theorem.

Theorem 1: Consider a vehicle with index $i_0 \in \{1, \dots, N_v - 1\}$ and all its follower vehicles $i \in \mathcal{I} = \{i_0 + 1, \dots, N_v\}$ satisfying the dynamics in (29). Then, there exists a control law $\tilde{a}_i = \phi(\tilde{x}_i, \tilde{x}_{i-1}) \in \mathcal{A}^f(\tilde{x}_i)$, for all $i \in \mathcal{I}$, such that for all $[\tilde{x}_{i-1}^T(t_0) \tilde{x}_i^T(t_0)]^T \in \mathcal{S}_i$ and $\tilde{a}_{i_0} \in \mathcal{A}^p(\tilde{x}_{i_0})$, the condition $[\tilde{x}_{i-1}^T(t) \tilde{x}_i^T(t)]^T \in \mathcal{S}_i$ holds for all $t \geq t_0$ and all $i \in \mathcal{I}$.

Proof: The application of Lemma 1 for $i = i_0 + 1$ proves the existence of an input $\tilde{a}_i \in \mathcal{A}^f(\tilde{x}_i)$ that ensures that $[\tilde{x}_{i-1}^T(t) \tilde{x}_i^T(t)]^T \in \mathcal{S}_i$ for all $t \geq t_0$. Then, by noting that $\mathcal{A}^f(\tilde{x}_i) \subseteq \mathcal{A}^p(\tilde{x}_i)$ according to (33b), it follows that $\tilde{a}_i \in \mathcal{A}^p(\tilde{x}_i)$. The result then follows by induction over the vehicle index, hereby repetitively applying Lemma 1. \square

This result is adapted to the MPC formulation in order to guarantee the safety of the platoon. More precisely, each vehicle, knowing the assumed state trajectory of the vehicle ahead, can compute the safety set for its own predicted state. By taking into account that the real state of the preceding vehicle is known with a one step delay, the safety set \mathcal{S}_i translates to the following safety constraints on each follower vehicle state:

$$s_i(t_{j+1}|t_k) - \frac{v_i^2(t_{j+1}|t_k)}{2\bar{a}_{\min,i}} \leq \hat{s}_{i-1}(t_{j-1}|t_k) - \frac{\hat{v}_{i-1}^2(t_{j-1}|t_k)}{2\bar{a}_{\min,i-1}} - l_{i-1} \quad (41a)$$

$$s_i(t_{j+1}|t_k) \leq \hat{s}_{i-1}(t_{j-1}|t_k) - l_{i-1} \quad (41b)$$

for $i = 2, \dots, N_v$. Note that the use of the predicted state at one step ahead $x_i(t_{j+1}|t_k)$ is due to the discrete nature of MPC; the use of the assumed trajectory of the preceding vehicle at one step behind $\hat{x}_{i-1}(t_{j-1}|t_k)$ is due to the delay in communication [modeled in the assumed trajectory definition (24)]. The constraints (41a) and (41b) correspond to the boundaries of \mathcal{S}_i characterized by g_1 and g_2 , respectively, as defined in (35). The constraints corresponding to g_3 and g_4 have been omitted here since they simply state that the vehicles should drive in the forward direction, which is true by assumption. We remark that, for safety purposes, only the safety constraints for $j = k$ is necessary. In fact it guarantees that, if at the update time t_k the current state of each follower vehicle is safe, then it is going to be safe also at the update time t_{k+1} . However, the safety constraints for $j > k$ give optimal trajectories that are safe over the whole horizon and therefore produce a smoother and more fuel-efficient behavior of the platoon. In the MPC formulation, we refer to the safety constraints (41a) and (41b) as $f_{\text{safe}}(x_i(t_{j+1}|t_k)) \geq 0$. The combination between this hard safety constraint and the soft no braking constraint (27) guarantees that braking occurs only when safety is compromised (i.e., the safety constraint is activated).

D. Cost Function

The objective of the vehicle control layer is to follow the optimal trajectory and the gap policy requirement provided by the platoon coordinator layer. This can be formulated by introducing the following cost function:

$$\begin{aligned} J_i^{\text{MPC}}(x_i(\cdot|t_k), a_i(\cdot|t_k), \epsilon_i(\cdot|t_k)) \\ = \sum_{j=k}^{k+H_{\text{MPC}}-1} \|x_i(t_j|t_k) - \hat{x}_{i-1}(t_{j-T_i}|t_k)\|_{\zeta_i Q}^2 \\ + \|x_i(t_j|t_k) - \bar{x}_i(t_j|t_k)\|_{(1-\zeta_i)Q}^2 \\ + \|a_i(t_j|t_k) - \bar{a}_i(t_j|t_k)\|_R^2 \\ + \|\epsilon_i(t_j|t_k)\|_P^2 \end{aligned}$$

where

$$\zeta_i = \begin{cases} 0, & \text{if } i = 1 \\ \bar{\zeta}, & \text{if } i = 2, \dots, N_v \end{cases} \quad (42)$$

and T_i represents the discretized version of the time gap τ_i (i.e., $T_i = \lfloor \tau_i / \Delta t_{\text{MPC}} \rfloor$). The parameters Q , R , and $\bar{\zeta} \in [0, 1]$ can be chosen in order to have a good tradeoff between reference trajectory, gap policy tracking, and actuators excitation. The weight P related to the softening variable of the constraint (27) is chosen relatively large such that only the activation of the safety constraint $f_{\text{safe}}(x_i(t_{j+1}|t_k)) \geq 0$ can result in a significant braking force.

E. MPC Formulation

We now have all the elements to formulate the MPC problem

$$\min_{a_i(\cdot|t_k), \epsilon_i(\cdot|t_k)} J_i^{\text{MPC}}(x_i(\cdot|t_k), a_i(\cdot|t_k), \epsilon_i(\cdot|t_k)) \quad (43a)$$

$$\text{s.t. } x_i(t_{j+1}|t_k) = Ax_i(t_j|t_k) + Ba_i(t_j|t_k) \quad (43b)$$

$$a_i(t_j|t_k) \in \mathcal{A}_i(x_i(t_j|t_k)) \quad (43c)$$

$$a_i(t_j|t_k) + \epsilon_i(t_j|t_k) \in \mathcal{A}_{\epsilon,i}(x_i(t_j|t_k)) \quad (43d)$$

$$v_i(t_j|t_k) \in \mathcal{V}(s_i(t_j|t_k)) \quad (43e)$$

$$f_{\text{safe}}(x_i(t_{j+1}|t_k)) \geq 0, \text{ if } i \geq 2 \quad (43f)$$

$$\epsilon_i(t_j|t_k) \geq 0 \quad (43g)$$

$$x_i(t_k|t_k) = x_i(t) \quad (43h)$$

where $j = k, \dots, k + H_{\text{MPC}} - 1$ and (43h) represents the initial condition of the MPC problem. For implementation purposes, the state-dependent constraint set in (43c), (43d), and (43e) will be replaced, respectively, by $\mathcal{A}_i(\hat{x}_i(t_j|t_k))$, $\mathcal{A}_{\epsilon,i}(\hat{x}_i(t_j|t_k))$, and $\mathcal{V}(\hat{s}_i(t_j|t_k))$. Taking into account that the safety constraint (43f) is quadratic and convex, the MPC problem can be recasted into a quadratic constraint quadratic programming problem for which efficient solvers exist.

The output of the vehicle controller is the desired acceleration $a_i^*(t_k)$ [defined as $a_i^*(t_k) = a_i^*(t_k|t_k)$, where $a_i^*(\cdot|t_k)$ is the optimal input trajectory resulting from the MPC] and a Boolean variable $a_{\text{br},i}$ defined as

$$a_{\text{br},i} = \begin{cases} 1, & \text{if } a_i^*(t_k) < a_{c,i}^*(t_k|t_k) \\ 0, & \text{if } a_i^*(t_k) \geq a_{c,i}^*(t_k|t_k) \end{cases} \quad (44)$$

which indicates if the desired acceleration defines a traction or a braking force.

VII. PERFORMANCE ANALYSIS OF THE PLATOON COORDINATOR

In this section, we analyze the performance of the platoon coordinator (as presented in Section V and shown in Figs. 6 and 7) by focusing on fuel efficiency. We compare its performance with other standard controller setups. To make the analysis independent of the low-level tracking strategy, we assume in this section that the vehicles can follow exactly the speed trajectories and spacing policies defined by the high-level controllers. The integrated system is evaluated in Section IX.

A. Experiment Setup

The comparison is done by using as benchmark the scenario introduced in Section II. We consider a platoon of two heavy-duty vehicles driving over the 45-km road stretch shown in Fig. 1 and investigate the controller performance for both homogeneous and heterogeneous platoons. The performance metrics chosen to compare the control configurations are the energy and the fuel consumed by each vehicle. In some comparisons, the consumed energy is preferred over the consumed fuel because it can be directly related to the energies dissipated by the various forces (i.e., gravitational, rolling, drag, and braking forces).

The control configurations analyzed in the comparisons are three control strategies and three gap policies. The following control strategies are considered.

- 1) *CC*: The first vehicle keeps the constant reference speed v_{CC} on low-grade slopes. If the uphill slope is too large to maintain constant speed, the engine generates the maximum power $P_{max,i}$ until the speed reaches v_{CC} again. If the downhill slope is too large to maintain a constant speed without braking, the engine coasts (i.e., does not inject any fuel, generating therefore the minimum power $P_{min,i}$) until the speed reaches v_{CC} again. However, if the vehicle reaches the speed limit v_{max} , the brakes are activated in order not to overcome it.
- 2) *LAC*: The first vehicle exploits the slope information of the road ahead in order to minimize its own fuel consumption.
- 3) *CLAC*: The first vehicle follows the speed profile generated by the platoon coordinator proposed in this paper.

The following gap policies are considered.

- 1) *Space Gap*: The second vehicle keeps a constant distance d_{SG} from the first vehicle.
- 2) *Headway Gap*: The second vehicle keeps a constant headway time τ_{HG} from the first vehicle, i.e., it keeps a distance proportional to its speed ($d_{HG}(t) = \tau_{HG}v_i(t)$).
- 3) *Time Gap*: The second vehicle keeps a constant time gap τ_{TG} from the first vehicle according to (12).

In order to maintain exactly the desired gap policies, the second vehicle is allowed to overcome the theoretical maximum engine power $P_{max,i}$ and to brake if necessary. In addition,

TABLE I
VEHICLE PARAMETERS

| Parameter | Value |
|--|--------------------|
| mass (m_i) | 40 t |
| length (l_i) | 18 m |
| rolling resistance coefficient (c_r) | 3×10^{-3} |
| vehicle cross-sectional area (A_v) | 10 m^2 |
| maximum engine power ($P_{max,i}$) | 298 kW |
| minimum engine power ($P_{min,i}$) | -9 kW |

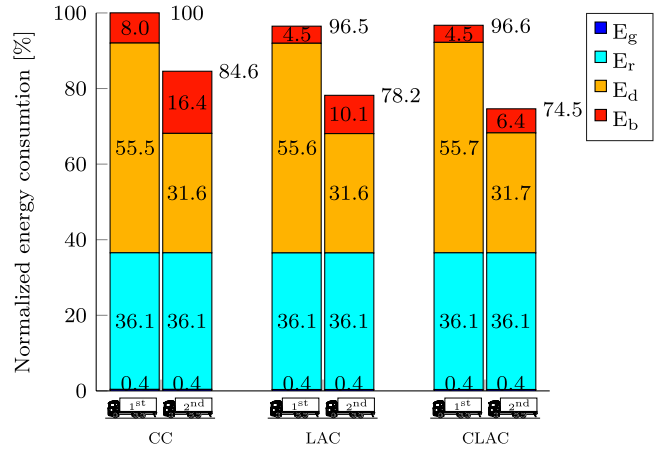


Fig. 9. Comparison of the energy consumed by each vehicle of a platoon ($m_1 = m_2 = 40 \text{ t}$) for the three control strategies, namely, CC, LAC, and CLAC, while keeping a time gap policy, driving over the 45-km road displayed in Fig. 1. Each bar represents the consumed energy normalized with respect to the energy consumed by a single vehicle driving alone using CC. The consumed energy is split into various components representing the energy dissipated by each force, namely, the gravitational (E_g), rolling (E_r), drag (E_d), and braking (E_b) forces.

in order to obtain a fair comparison, it is ensured, by tuning the tradeoff parameter β of the LAC and CLAC formulations [see (42)], that the control strategies have the same average speed \bar{v} and the parameters d_{SG} , τ_{HG} , and τ_{TG} are chosen such that the vehicles, despite the different gap policies, have the same distance when driving at constant speed \bar{v} (i.e., $d_{SG} = \bar{v}\tau_{HG} = \bar{v}\tau_{TG} - l_1$). Furthermore, in order to remove the influence of the residual kinematic energy, the initial and final speeds are constrained to be the same in all the controller configurations.

B. Fuel-Efficiency Analysis for Control Strategies

In this section, we present the results of the platoon behavior for the three control strategies, while keeping a time gap policy ($\tau_{TG} = 1.4 \text{ s}$). In the first part, as in the motivational experiment of Section II, we focus on the homogeneous platoon scenario, while in the second part, we consider two heterogeneous platoons (i.e., platoons where the second vehicle is, respectively, heavier and lighter than the leading one).

We now consider a platoon of two identical vehicles, whose parameter values are displayed in Table I. We start the comparison by analyzing the comprehensive bar diagram displayed in Fig. 9 representing the energy consumed by each vehicle of the platoon for the three control strategies (the corresponding fuel consumption is displayed in the middle column of Table II). The consumed energy is split into

TABLE II

NORMALIZED FUEL CONSUMPTION (%) OF THE PLATOONING VEHICLE FOR DIFFERENT CONTROL STRATEGIES AND SCENARIOS (VEHICLE WEIGHTS). THE FUEL IS NORMALIZED WITH RESPECT TO THE FUEL CONSUMED BY THE CORRESPONDING VEHICLE DRIVING ALONE USING CC

| mass | 1st | | 2nd | | 1st | | 2nd | |
|------|-------|------|-------|------|-------|------|-------|------|
| | 35 t | 45 t | 40 t | 40 t | 45 t | 35 t | 40 t | 45 t |
| CC | 100.0 | 90.2 | 100.0 | 86.3 | 100.0 | 82.1 | 100.0 | 90.2 |
| LAC | 97.6 | 84.9 | 96.9 | 80.6 | 96.3 | 77.2 | 97.6 | 84.9 |
| CLAC | 97.8 | 78.0 | 97.0 | 77.4 | 96.4 | 76.7 | 97.8 | 78.0 |

various components representing the energy dissipated by each force, namely, the gravitational, rolling, drag, and braking forces. We first notice how the second vehicle, for all control strategies, consumes less energy compared with the first one, due to the significant reduction of the energy associated with the drag force. Second, comparing the three control strategies, we can observe how the use of the LAC allows both vehicles to save energy, respectively, 3.5% and 6.4% compared with the use of the CC. Instead, by switching from the LAC to the CLAC, the first vehicle consumes 0.1% more energy, while the second one saves 3.7% of energy; therefore, the platoon, given by the union of the two vehicles, saves 3.6% of energy. This result is in line with our expectation, since the LAC optimizes the fuel consumption of the first vehicle, while the CLAC targets the reduction of the fuel consumption of the entire platoon. Consequently, the savings of the CLAC strategy with respect to the LAC strategy are expected to increase for platoons of more than two vehicles. Going into the details of the various consumed energy components, first we notice that the gravitational and rolling energy components are the same for both vehicles for all the considered control strategies. This is due to the fact that the energy associated with the gravitational force depends only on the difference of altitude between the initial and final points, while the rolling energy only depends on the driven distance, which is the same by experiment design specification. The drag energy, instead, is significantly different for the two vehicles because of its dependence on the distance to the preceding vehicle, while it is approximately the same for the different control strategies. What significantly changes between the different control strategies is the energy dissipated by braking.

In order to understand the role of the control strategies in the use of brakes, in Fig. 10, we show part of the simulation results corresponding to the road highlighted as Sector B in Fig. 1. In this paper, we have chosen to focus on a downhill section because this is where the braking action is taking place. The comparison of the platoon behaviors follows.

- 1) **CC:** During the downhill, starting from speed v_{CC} , the first vehicle accelerates while coasting due to the large road grade. In the meantime, the second vehicle has to brake slightly in order to maintain the time gap and compensate for the reduced drag force compared with the first vehicle. At 38.1 km, in order not to overcome the speed limit, both vehicles need to brake significantly.

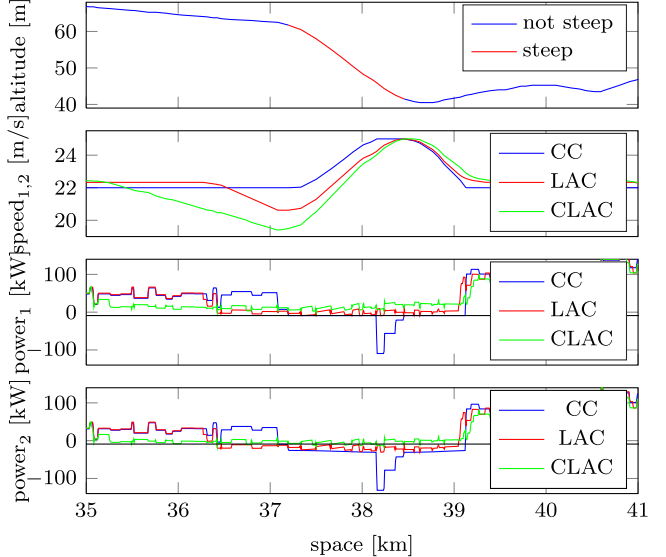


Fig. 10. Comparison of the behavior of a homogeneous platoon (i.e., $m_1 = m_2 = 40 \text{ t}$) for three different control strategies, namely, CC, LAC, and CLAC, while keeping a time gap policy and driving over Sector B displayed in Fig. 1. First plot: the road altitude. Second plot: the speed profiles for the three control strategies followed by both vehicles (because of the time gap policy). Third and forth plots: the summation between the power generated by the engine and the braking systems for the two vehicles and three control strategies. Black lines: the theoretical minimum and maximum engine power, respectively, $P_{\min,i}$ and $P_{\max,i}$ (hence, if the power crosses the lower power limit $P_{\min,i}$, the corresponding vehicle is braking).

- 2) **LAC:** By exploiting the topography information of the road ahead, the first vehicle reduces its speed before the downhill by anticipating the coasting phase such that the speed limit is reached only when the slope grade is small enough to stop accelerating while coasting and therefore it avoids braking. The second vehicle, as in the CC case, has to brake slightly while the first vehicle is coasting but it also avoids the significant braking phase at the end of the downhill.
- 3) **CLAC:** Since in this case the optimization is done considering the fuel consumption of both vehicles, the first vehicle starts to lose speed earlier before the downhill. This allows it to slightly throttle during the downhill, allowing the second vehicle to coast meanwhile and, as in the LAC case, to reach the speed limit only when the slope grade is small enough to stop accelerating while coasting. In this case, no vehicle has to brake.

Note that, in the case of longer downhill segments, the lower speed bound does not allow the vehicle to decrease the speed enough before the downhill in order not to hit the upper speed limit during the downhill. This is why in some sections of the 45-km benchmark road, in the LAC case, the first vehicle and, in the CLAC case, both vehicles still need to brake.

So far, we have considered the case of a homogeneous platoon. What we want to investigate now is the role of the control strategies in the case of heterogeneous platoons. In Table II, we report the normalized fuel consumption for the cases of two heterogeneous platoons and the homogeneous platoon previously considered. The vehicles have the same powertrain, but their masses vary between 35, 40, and 45 tons.

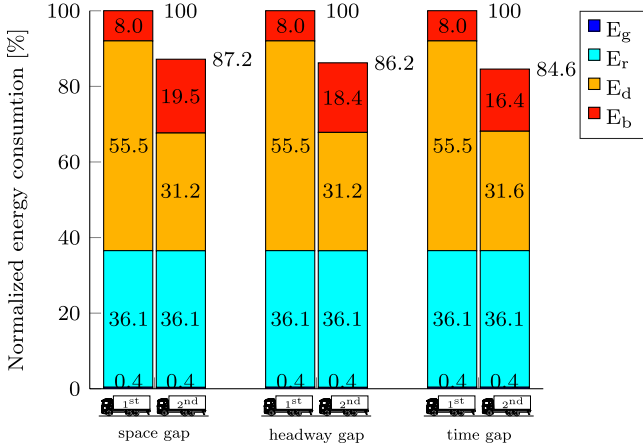


Fig. 11. Comparison of the energy consumed by each vehicle of a homogeneous platoon ($m_1 = m_2 = 40 t$) for three different gap policies, namely, space, headway, and time gap policies, while using CC as control strategy and driving over the 45-km road displayed in Fig. 1. For detailed explanation refer to the caption of Fig. 9.

Analyzing Table II, we can notice how in the case of a heavier second vehicle the CLAC allows one to save 10.8% of fuel compared with the CC, while, in the case of a lighter second vehicle, it allows one to save 5.4%. However, from the last row we note that, with the use of the CLAC, the order of the vehicles does not significantly change the normalized fuel consumption.

In conclusion, the proposed CLAC has a significant impact on the reduction of the energy and fuel consumption. The majority of the fuel saving is related to the reduction of energy dissipated by braking during the downhill sections. The impact of such a controller grows in the case of a heavier follower vehicle.

C. Fuel-Efficiency Analysis for Gap Policies

In the previous analysis, we have considered a time gap policy. The aim of this section is to compare the platoon performance for different gap policies, namely, space, headway, and time gap policies, while keeping the same control strategy (in the analysis we have chosen CC). Note that in order to be able to follow the required gap policy the second vehicle is allowed to exceed the maximum engine power. In this section, we focus on a homogeneous platoon, since the results for a heterogeneous platoon are qualitatively the same. In Fig. 11, we show the comprehensive bar diagram representing the normalized energy consumed by each vehicle in the platoon for the three gap policies, while using CC as control strategy. Since the first vehicle uses the same control strategy, the energy consumption differs only for the second vehicle. It is interesting to notice that, similar to the comparisons done in the previous section, the main difference between the energy consumption of the second vehicle is related to the energy dissipated by braking. The headway gap policy allows the second vehicle to save 1% over the space gap policy, while the time gap policy allows one to save an additional 1.6% of energy. In order to understand the role of the gap policy on the braking energy, we show the platoon behavior driving over a synthetic hill composed of an uphill section with constant

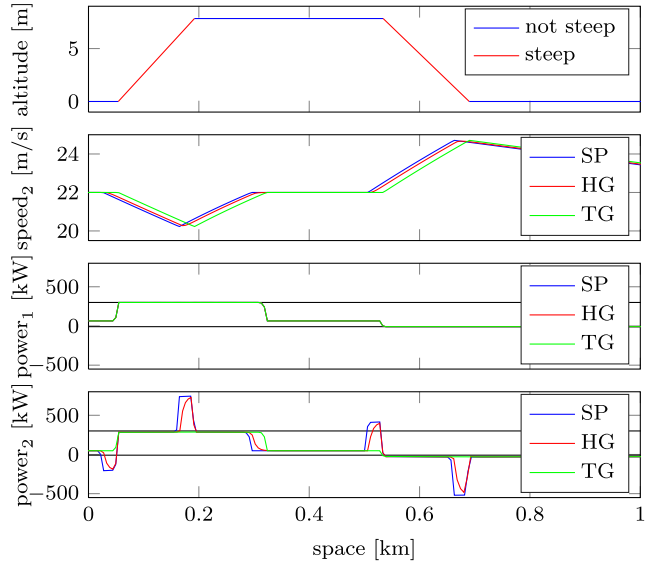


Fig. 12. Comparison of the behavior of a homogeneous platoon (i.e., $m_1 = m_2 = 40 t$) for three different gap policies, namely, space gap (SG), headway gap (HG), and time gap (TG) policies, while using CC as control strategy and driving over a synthetic hill. For the explanation of plots, refer to the caption of Fig. 10; note that the second plot shows only the speed trajectories of the second vehicle (the speed trajectory of the first vehicle coincides with that one of the second vehicle in the case of time gap policy).

slope grade, a flat section, and a downhill section with constant slope grade. The platoon behavior for such a hill is shown in Fig. 12. Analyzing the second vehicle's behavior for each gap policy, the following can be observed.

- 1) *Time Gap Policy:* As argued in Section V, the time gap allows the vehicles to follow the same speed profile over space. That means that the generated forces, and therefore, the generated powers (because of the equal speed result) are equivalent except for a reduction of the air drag component in the second vehicle. Therefore, the power generated by the second vehicle, as can be observed in Fig. 12, is approximately a biased equivalent of the power generated by the first vehicle. As a result, the second vehicle complies with the limitation on maximum engine power.
- 2) *Space Gap Policy:* The space gap requires the vehicles to follow the same speed profile over time. An interesting consequence can be observed, for example, at the beginning of the uphill section shown in Fig. 12; as soon as the first vehicle enters the uphill section and decelerates because of limited engine power, the second vehicle, which is still in the flat section, has to brake in order to respect the space gap requirement. In general, excluding the offset given by the drag power, every time the slope increases (in Fig. 12, entering the uphill and leaving the downhill sections), the second vehicle has to generate less power than the first vehicle, while every time the slope decreases (in Fig. 12, leaving the uphill and entering the downhill sections) the second vehicle has to generate more power than the first vehicle. As a consequence, the second vehicle has, respectively, to brake and to exceed the power limit in order to follow the required space gap policy.

TABLE III

NORMALIZED FUEL CONSUMPTION (%) OF THE PLATOONING VEHICLES FOR DIFFERENT CONTROL STRATEGIES AND GAP POLICIES. THE FUEL IS NORMALIZED WITH RESPECT TO THE FUEL CONSUMED BY THE RESPECTIVE VEHICLE DRIVING ALONE USING CC

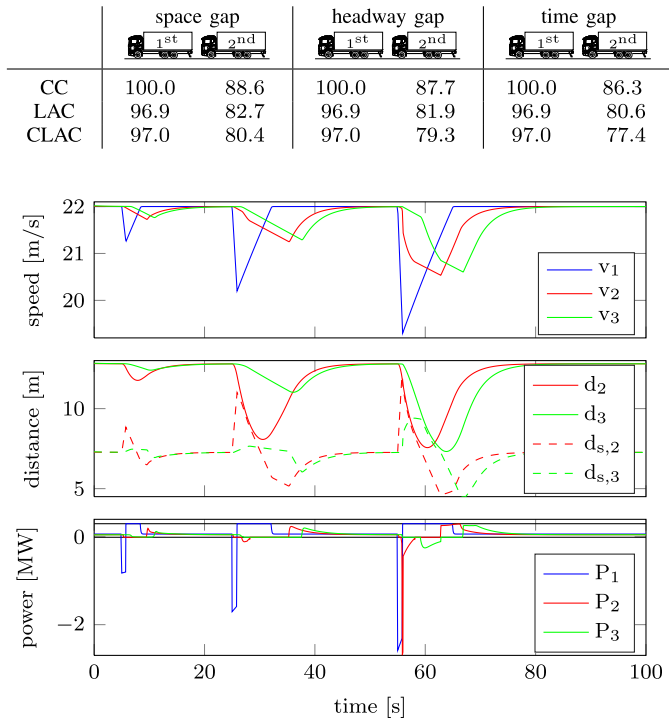


Fig. 13. Behavior of a three identical vehicles platoon driving on a flat road. The leading vehicle brakes three times at 5, 25, and 55 s, with a braking deceleration of 1, 2, and 3 m/s^2 , respectively, for 0.9 s. First plot: the speed of the three vehicles. Second plot: the distance between the vehicles and the corresponding safety distance computed using an adaptation of inequality (41b). Third plot: the summation between the power generated by the engine and the braking systems of the vehicles.

3) *Headway Gap Policy:* The headway gap can be considered as a tradeoff between a time gap and a space gap. For example, as soon as the first vehicle enters the uphill section and starts to decelerate, the distance between the two vehicles is allowed to decrease, but this decrease is not as fast as in the case of the time gap.

The results obtained by the analysis of the platoon behavior in the case of the synthetic hill are also valid in the case of the original scenario. In conclusion, the time gap allows one to save more energy compared with the space and headway gaps. In addition, the time gap allows all the vehicles to follow the same speed trajectory in space and, therefore, it scales well with the number of vehicles in the platoon. The complete results for the normalized fuel consumption are reported in Table III.

VIII. PERFORMANCE ANALYSIS OF THE VEHICLE CONTROLLER

In this section, we analyze the performance of the vehicle control layer (as presented in Section VI and shown in Figs. 6 and 7) by focusing on the safety aspect. The analysis is based on the simulation result displayed in Figs. 13 and 14, where the leading vehicle of a three-vehicle platoon driving on a flat road brakes repeatedly with different braking profiles.

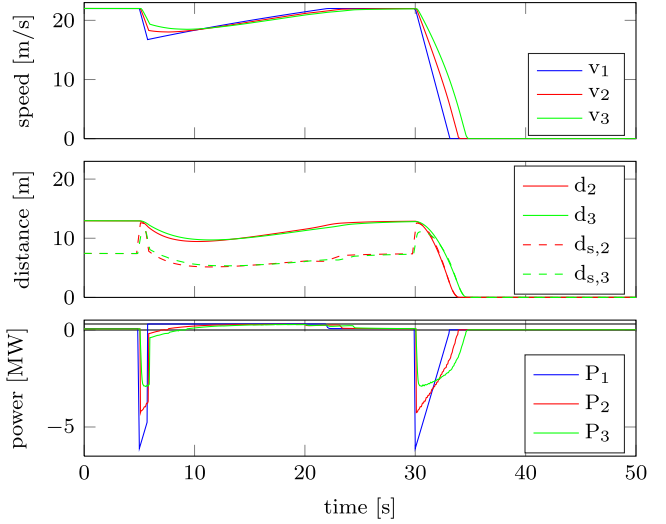


Fig. 14. Behavior of a three identical vehicles platoon driving on a flat road. The leading vehicle brakes a first time at 5 s for 1 s with a deceleration of 7 m/s^2 and a second time at 25 s with a deceleration of 7 m/s^2 until arriving to full stop. For the plot explanation refer to the caption of Fig. 13.

Here, we assume that the leading vehicle is manually driven in the braking phases and, therefore, the control system does not have *a priori* knowledge about the braking profile. The considered vehicles are identical with the parameter values defined in Table I.

A. Safety Analysis

Here, we focus on the safety analysis of the distributed vehicle control layer and, in particular, we analyze the role of the safety constraint in various situations. In Fig. 13, the leading vehicle is braking with deceleration of 1, 2, and 3 m/s^2 for 0.9 s at 5, 25, and 55 s, respectively. In the second plot of Fig. 13, the effective distances and the ones that would activate the safety constraint (we will refer to it as the safety distance) are shown. First, we can notice how, in line with our expectation, the second and the third vehicle are braking (see the third plot) only when the effective distance touches the safety distance. In fact here we recall that, according to how the vehicle controller is designed (see Section VI-E), only the activation of the safety constraint or a braking request from the platoon coordinator can lead to a significant braking action. Consequently, during the first braking instance of 1 m/s^2 , both follower vehicles do not brake, despite the deviation of their states from the reference trajectories. During the second braking of 2 m/s^2 , instead, the safety constraint of the second vehicle is activated and therefore it requires a braking action. Finally, during the third braking of 3 m/s^2 , the safety constraints of both follower vehicles activate and therefore they both brake. Note that the safety constraint is designed such that fuel efficiency has priority on driver comfort. In fact, in this case, in order to be fuel efficient, the braking action is required only when the platoon is in a safety-critical situation. However, *a priori* knowledge of the braking profile of the first vehicle (e.g., by having a model of the driver or handling the braking action autonomously) would enable a smoother and less intense braking action.

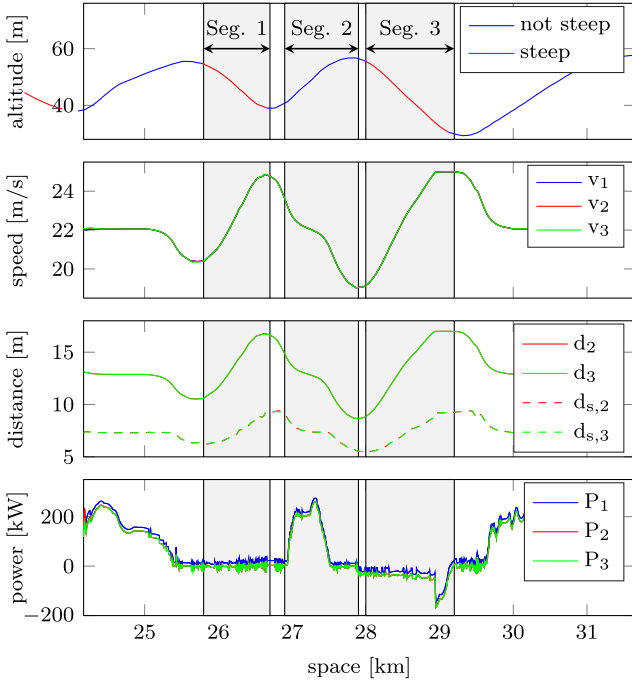


Fig. 15. Simulation results obtained using the proposed controller for a three-vehicle platoon while driving over Sector A highlighted in Fig. 1. The three vehicles are identical with parameters shown in Table I. First plot: the road topography. For the explanation of the other plots refer to the caption of Fig. 13.

In Fig. 14, we consider a more challenging scenario in which the first vehicle brakes with higher intensity, simulating an emergency situation. More precisely, it brakes at 5 s with a deceleration of 7 m/s^2 for 1 s and at 30 s with the same deceleration until it arrives to full-stop. We can notice how, also in this scenario, the safety constraint in each vehicle control layer activates the braking action and guarantees that no collision occurs between the vehicles.

IX. PERFORMANCE ANALYSIS OF THE INTEGRATED SYSTEM

In this section, we analyze the simulation results displayed in Fig. 15 of the platoon under the control of the integrated control architecture, i.e., including both the platoon coordinator and the vehicle control layer. More precisely, in this analysis we consider a platoon of three identical vehicles (whose parameters are defined in Table I) driving over Sector A highlighted in Fig. 1. This is the same sector for which the experimental results in [19] are displayed in Fig. 2 and analyzed in Section II.

At first glance, as expected from the platoon coordinator formulation, we can notice how all the vehicles follow the same speed and distance profiles in the spacial domain. In addition, in order to follow such profiles, we observe in the last plot how the second and the third vehicle, thanks to the air drag reduction, need to generate less power than the leading vehicle. We now continue the analysis by focusing on the three critical segments highlighted in Fig. 15.

- 1) *Segment 1:* Due to the steep downhill, all vehicles are not able to maintain the constant speed without braking and,

therefore, they accelerate. However, the platoon coordinator requires the leading vehicle to throttle slightly such that the follower vehicles can coast. In this case, the coordination role of the platoon coordinator allows one to avoid braking action to all vehicles, hereby ensuring a lower overall fuel consumption.

- 2) *Segment 2:* Since no gearshift is taken into account, the vehicles are able to maintain the time gap requirement during the uphill.
- 3) *Segment 3:* Due to the longer downhill compared with the one of Segment 1, the platoon exhibits a different behavior. First, the platoon coordinator requires all vehicles to decrease the speed to the minimum allowed (in this simulation it is set to 19 m/s) in order to hit the maximum speed limit as late as possible. Second, since the speed limit is reached despite the decrease of speed at the beginning of the downhill, the platoon coordinator requires the first vehicle to coast and the follower vehicles to brake slightly to maximize the efficiency. In fact, in this case, to require the first vehicle to slightly throttle in the first part of the downhill section and brake at its end would be contradictory and lead to increased fuel consumption.

In conclusion, the platoon with the integrated control architecture shows a fuel efficient and smooth behavior.

X. CONCLUSION

In this paper, we have presented a novel control architecture based on LAC for fuel-efficient and safe heavy-duty vehicle platooning. The use of an LAC framework for truck platooning has been first motivated by the analysis of real experiments. In particular in this analysis we concluded that the use of topography information in order to predict the behavior of the vehicles and coordination between the vehicles can be beneficial for both fuel efficiency and safety reasons. This led to a control architecture divided into two layers. A centralized higher layer, denoted as platoon coordinator, is responsible for the coordination of the platoon by defining a speed profile that is feasible and fuel efficient for the entire platoon by exploiting preview topography information. This speed profile is communicated to each block of the decentralized lower layer, denoted as vehicle control layer. Within each vehicle controller an MPC routine tracks the reference speed profile and gap policy and generates the real-time desired acceleration for the vehicle engine and braking management systems, while guaranteeing safety. The performance of the proposed platoon controller has been evaluated through the analysis of numerical experiments. The performance of the two control layers has been studied both separately and in conjunction.

In the modeling of the vehicle powertrain, we have assumed that the gear ratio can be chosen over a continuous interval. However, this is not typically the case in commercial trucks, where usually the transmission is handled by a gearbox that introduces fixed gear ratios and power losses during the gearshifts. Therefore, in future work, we want to investigate how the presence of a gearbox should be managed in an optimal way. The optimal engine speed as function of the

generated power shown in Fig. 5 and the knowledge of the current speed can be used to compute the instantaneous optimal gear ratio. However, the power loss and the delay during the gearshift make the problem of when the vehicles should change gear (e.g., independently or simultaneously) and which gear they should engage not trivial. Second, we would like to investigate how external disturbances, as traffic ahead or a vehicle cutting in the platoon, can be handled in an autonomous way within the platoon controller framework. So far, in fact, such disturbances have been assumed to be handled manually by the drivers. However, the prediction of local traffic would allow the platoon to move fuel efficiently and safely.

ACKNOWLEDGMENT

The authors would like to thank Dr. A. Alam and Dr. H. Pettersson from Scania for the fruitful discussions and for providing the motivating experiment data.

REFERENCES

- [1] *EU Transport in Figures—Statistical Pocketbook*, Eur. Commission, Brussels, Belgium, 2014.
- [2] N. Hill *et al.*, “Reduction and testing of greenhouse gas emissions from heavy duty vehicles,” AEA Technol. Inc., Carlsbad, CA, USA, Tech. Rep. AEA/ED46904, 2011.
- [3] *ITF Transport Outlook*, Int. Transport Forum, OECD, Paris, France, 2015.
- [4] *Roadmap to a Single European Transport Area: Towards a Competitive and Resource Efficient Transport System*, Eur. Commission, Brussels, Belgium, 2011.
- [5] *EPA and NHTSA Adopt First-Ever Program to Reduce Greenhouse Gas Emissions and Improve Fuel Efficiency of Medium- and Heavy-Duty Vehicles*, U.S. Environ. Protection Agency, Washington, DC, USA, Aug. 2011.
- [6] *Annual Report 2013*, Scania AB, Södertälje, Sweden, Aug. 2013.
- [7] E. Hellström, “Look-ahead control of heavy vehicles,” Ph.D dissertation, Dept. Elect. Eng., Linköping Univ., Linköping, Sweden, 2010.
- [8] C. Bonnet and H. Fritz, “Fuel consumption reduction in a platoon: Experimental results with two electronically coupled trucks at close spacing,” SAE Tech. Paper 724, 2000.
- [9] F. Browand, J. McArthur, and C. Radovich, “Fuel saving achieved in the field test of two tandem trucks,” Inst. Transp. Stud., UC California, Berkeley, CA, USA, Tech. Rep. UCB-ITS-PRR-2004-20, Jun. 2004.
- [10] M. P. Lammert, A. Duran, J. Diez, K. Burton, and A. Nicholson, “Effect of platooning on fuel consumption of Class 8 vehicles over a range of speeds, following distances, and mass,” *SAE Int. J. Commercial Vehicles*, vol. 7, no. 2, pp. 626–639, Sep. 2014.
- [11] A. Alam, J. Mårtensson, and K. H. Johansson, “Experimental evaluation of decentralized cooperative cruise control for heavy-duty vehicle platooning,” *Control Eng. Pract.*, vol. 38, pp. 11–25, May 2015.
- [12] L. E. Peppard, “String stability of relative-motion PID vehicle control systems,” *IEEE Trans. Autom. Control*, vol. 19, no. 5, pp. 579–581, Oct. 1974.
- [13] W. B. Dunbar and R. M. Murray, “Distributed receding horizon control for multi-vehicle formation stabilization,” *Automatica*, vol. 42, no. 4, pp. 549–558, Apr. 2006.
- [14] G. J. L. Naus, R. P. A. Vugts, J. Ploeg, M. J. G. van de Molengraft, and M. Steinbuch, “String-stable CACC design and experimental validation: A frequency-domain approach,” *IEEE Trans. Veh. Technol.*, vol. 59, no. 9, pp. 4268–4279, Nov. 2010.
- [15] S. E. Shladover, “PATH at 20—History and major milestones,” *IEEE Trans. Intell. Transp. Syst.*, vol. 8, no. 4, pp. 584–592, Dec. 2007.
- [16] C. Bergenhem, Q. Huang, A. Benmimoun, and T. Robinson, “Challenges of platooning on public motorways,” in *Proc. 17th ITS World Congr.*, Busan, South Korea, 2010, pp. 1–12.
- [17] C. Bergenhem, H. Pettersson, E. Coelingh, C. Englund, S. Shladover, and S. Tsugawa, “Overview of platooning systems,” in *Proc. 19th ITS World Congr.*, Vienna, Austria, 2012, pp. 1–8.
- [18] S. E. Shladover, “Recent international activity in cooperative vehicle-highway automation systems,” California PATH, Richmond, CA, USA, Tech. Rep. FHWA-HRT-12-033, 2012.
- [19] A. Alam, B. Besselink, V. Turri, J. Mårtensson, and K. H. Johansson, “Heavy-duty vehicle platooning for sustainable freight transportation: A cooperative method to enhance safety and efficiency,” *IEEE Control Syst. Mag.*, vol. 35, no. 6, pp. 34–56, Dec. 2015.
- [20] S. Tsugawa, “An overview on an automated truck platoon within the energy ITS project,” in *Proc. 7th IFAC Symp. Adv. Automotive Control*, Tokyo, Japan, 2013, pp. 41–46.
- [21] E. Hellström, M. Ivarsson, J. Åslund, and L. Nielsen, “Look-ahead control for heavy trucks to minimize trip time and fuel consumption,” *Control Eng. Pract.*, vol. 17, pp. 245–254, Feb. 2009.
- [22] A. Alam, J. Mårtensson, and K. H. Johansson, “Look-ahead cruise control for heavy duty vehicle platooning,” in *Proc. 16th Int. IEEE Conf. Intell. Transp. Syst.*, The Hague, The Netherlands, Oct. 2013, pp. 928–935.
- [23] B. Németh and P. Gáspár, “Optimised speed profile design of a vehicle platoon considering road inclinations,” *IET Intell. Transp. Syst.*, vol. 8, no. 3, pp. 200–208, May 2014.
- [24] A. Kaku, A. S. Kamal, M. Mukai, and T. Kawabe, “Model predictive control for ecological vehicle synchronized driving considering varying aerodynamic drag and road shape information,” *SICE J. Control, Meas., Syst. Integr.*, vol. 6, no. 5, pp. 299–308, 2013.
- [25] R. E. Bellman, *Dynamic Programming*. Princeton, NJ, USA: Princeton Univ. Press, 1957.
- [26] F. Borrelli, A. Bemporad, and M. Morari. (2015). *Predictive Control for Linear and Hybrid Systems*. [Online]. Available: <http://www.mpc.berkeley.edu/mpc-course-material>
- [27] V. Turri, B. Besselink, J. Mårtensson, and K. H. Johansson, “Fuel-efficient heavy-duty vehicle platooning by look-ahead control,” in *Proc. IEEE 53rd Annu. Conf. Decision Control*, Los Angeles, CA, USA, Dec. 2014, pp. 654–660.
- [28] V. Turri, “Fuel-efficient and safe heavy-duty vehicle platooning through look-ahead control,” licentiate thesis, KTH Royal Inst. Technol., Stockholm, Sweden, 2015.
- [29] W.-H. Hucho, *Aerodynamics of Road Vehicles*. Oxford, U.K.: Butterworth-Heinemann, 1987.
- [30] D. Norrby, “A CFD study of the aerodynamic effects of platooning trucks,” M.S. thesis, KTH Royal Inst. Technol., Stockholm, Sweden, 2014.
- [31] T. Sandberg, “Heavy truck modeling for fuel consumption simulations and measurements,” licentiate thesis, Dept. Elect. Eng., Linköping Univ., Linköping, Sweden, 2001.
- [32] G. F. Newell, “A simplified car-following theory: A lower order model,” *Transp. Res. B, Methodol.*, vol. 36, no. 3, pp. 195–205, 2002.
- [33] S. Öncü, J. Ploeg, N. van de Wouw, and H. Nijmeijer, “Cooperative adaptive cruise control: Network-aware analysis of string stability,” *IEEE Trans. Intell. Transp. Syst.*, vol. 15, no. 4, pp. 1527–1537, Aug. 2014.
- [34] J. I. Ge and G. Orosz, “Dynamics of connected vehicle systems with delayed acceleration feedback,” *Transp. Res. C, Emerg. Technol.*, vol. 46, pp. 46–64, Sep. 2014.
- [35] A. Alam, A. Gattami, K. H. Johansson, and C. J. Tomlin, “Guaranteeing safety for heavy duty vehicle platooning: Safe set computations and experimental evaluations,” *Control Eng. Pract.*, vol. 24, pp. 33–41, Mar. 2014.
- [36] F. Blanchini, “Set invariance in control,” *Automatica*, vol. 35, no. 11, pp. 1747–1767, Nov. 1999.



Valerio Turri received the M.Sc. (*cum laude*) degrees in control engineering from the Politecnico di Milano, Milan, Italy, and the Politecnico di Torino, Turin, Italy, in 2011. He is currently pursuing the Ph.D. degree with the ACCESS Linnaeus Centre, Department of Automatic Control, KTH Royal Institute of Technology, Stockholm, Sweden.

He was a Research Engineer with the Model Predictive Control Laboratory, Department of Mechanical Engineering, University of California at Berkeley, Berkeley, CA, USA, in 2012. His current research interests include model predictive control and its application to advanced automotive control.



Bart Besselink received the M.Sc. (*cum laude*) degree in mechanical engineering and the Ph.D. degree from the Eindhoven University of Technology, Eindhoven, The Netherlands, in 2008 and 2012, respectively.

He was a short-term Visiting Researcher with the Tokyo Institute of Technology, Tokyo, Japan, in 2012. He is currently a Post-Doctoral Researcher with the ACCESS Linnaeus Centre, Department of Automatic Control, KTH Royal Institute of Technology, Stockholm, Sweden. His current research interests include systems theory and model reduction for nonlinear dynamical systems and large-scale interconnected systems with applications in the field of intelligent transportation systems.



Karl H. Johansson (F'13) received the M.Sc. and Ph.D. degrees in electrical engineering from Lund University, Lund, Sweden.

He has held visiting positions with the University of California at Berkeley, Berkeley, CA, USA, the California Institute of Technology, Pasadena, CA, USA, Nanyang Technological University, Singapore, and the Institute of Advanced Studies, The Hong Kong University of Science and Technology, Hong Kong. He is currently the Director of the ACCESS Linnaeus Centre and a Professor with the School of Electrical Engineering, KTH Royal Institute of Technology, Stockholm, Sweden, where he heads the Stockholm Strategic Research Area ICT The Next Generation. His current research interests include networked control systems, cyber-physical systems, and applications in transportation, energy, and automation systems.

Dr. Johansson is a member of the IEEE Control Systems Society Board of Governors and the European Control Association Council. He received many honors, including Wallenberg Scholar by the Knut and Alice Wallenberg Foundation, Future Research Leader from the Swedish Foundation for Strategic Research, and Young Author Prize from International Federation of Automatic Control.